RUSSIAN JOURNAL OF EARTH SCIENCES, VOL. 5, NO. 2, PAGES 101–123, APRIL 2003

MAR volcanism in the Sierra Leone Fracture Zone region, Central Atlantic

S. G. Skolotnev, A. A. Peyve, and S. M. Lyapunov

Geological Institute of the Russian Academy of Sciences, Pyzhevsky pereulok 7, 119017 Moscow, Russia

V. A. Simonov, Yu. E. Glazyrin, and V. Yu. Kolobov

Joint Institute of Geology, Geophysics, and Mining, Siberian Branch of the Russian Academy of Sciences, prospekt Akademika Koptyuga 3, 630090 Novosibirsk, Russia

Abstract. We have studied major and trace element (including REE) geochemistries of basalts and chilled basaltic glasses from the MAR axial zone in the vicinity of the Sierra Leone FZ (5°–7°10′ N). The links of basalts of various compositions with particular ocean-floor geological structural features have been analyzed as well. Three basaltic varieties have been discriminated. Almost ubiquitous are high-Mg basalts that are derivatives of N-MORB tholeiitic melts and that are produced in the axial zone of spreading. Variety 2 is alkaline basalts widespread on the southwest flank of the MAR crestal zone in the Sierra Leone region, likely generated through deep mantle melting under plume impact. Variety 3 is basalts derivative from T- and P-MORB-like tholeiitic melts and originating through addition of a deeper mantle material to depleted upper mantle melts. Magma generation parameters, as calculated from chilled glass compositions, are different for depleted tholeiites (44–55 km, 1320–1370°C) and enriched tholeiites (45–78 km, 1330–1450°C). Mantle plume impact is shown to affect not only tholeiitic basalt compositions but also magma generation conditions in the axial spreading zone, resulting in higher Ti and Na concentrations in the melts parental to the rift-related basalts occurring near the plume. T- and P-MORBs are also developed near the areas where mantle plumes are localized. The high-Mg basalts are shown to come in several types with distinctive Ti and Na contents. Nearly every single MAR segment (bounded by sinistral strike slips and the Bogdanov FZ) is featured by its own basalt type suggesting that it has formed above an asthenospheric diapir with its unique magma generation conditions. These conditions are time variable. The likely causes of the temporal and spatial instability of mantle upwelling beneath this portion of the MAR are singular tectonic processes and plume activity. In the sulfide-bearing rift morphostructures (the so-called "Ore area" and the Markov Basin), basalts make up highly evolved suites generated through olivine and plagioclase fractionation, which is suggestive of relatively long-lived magma chambers beneath the sulfide-bearing rift morphostructures. The functioning of these chambers is a combined effect of a singular geodynamic regime and plume activity. In these chambers, melts undergo deep differentiation leading to progressively increasing concentration of the sulfide phase, eventually to be supplied to the hydrothermal plumbing system.

Paper number TJE03117.
ISSN: 1681–1208 (online)

The online version of this paper was published 3 June 2003.
URL: http://rjes.wdcb.ru/v05/tje03117/tje03117.htm

Introduction

This work discusses the results of our study on compositions of basalts and their chilled glasses recovered from the axial zone of the Mid-Atlantic Ridge (MAR) in the vicinity of the Sierra Leone FZ (Central Atlantic) during the

R/V Akademik Nikolaj Strakhov Cruise 22 and the R/V Akademik Ioffe Cruise 10. It is for three basic reasons that this particular MAR portion (hereinafter, the Sierra Leone region) has been a focus of geologic studies.

Firstly, prior to the above cruises this MAR segment remained among the least well understood portions of the Central Atlantic. In 1968, it was covered by several dredge hauls [*Bonatti,* 1968]. This exercise contributed considerably to filling in the existing gap in the bathymetry of the MAR axial zone in the Central Atlantic.

Secondly, judging from satellite altimetry maps [*Sandwell and Smith,* 1997], the Sierra Leone region (which includes the MAR axial part between 5°N and 7°10′ N) separates two structurally distinct MAR domains. North of the Bogdanov FZ, the MAR rift valley is cut by major transform faults (Doldrums, Vernadsky, Arkhangelsky, etc.) [*Pushcharovsky et al.,* 1992] into short NS trending segments. A setup like this is typical of slow spreading ridges such as the MAR. South of 5°N, by contrast, the rift valley and its rimming MAR structures (stretching as far as the Strakhov FZ) trend clearly NS without showing evidence of an offset. The ridge flanks are level plateaus with thick sedimentary cover [*Udintsev et al.,* 1996].

Thirdly, this MAR segment is in a low seismic activity area. The most hydrothermal fields known to date within the MAR are confined to such areas [*Mazarovich and Sokolov,* 1998]. The forecast advanced by A. O. Mazarovich and S. Yu. Sokolov was fully validated in the course of the cruise surveys juts mentioned. In the vicinity of the survey area, three localities were discovered that have potentials for massive sulfide mineralization, existing or being formed, in zones of discharge of high-temperature fluids. The most promising among them is the Markov rift basin. On its eastern slope, non-oxidized massive sulfides consisting mainly of chalcopyrite, as well as sulfide-bearing wallrock metasomatites, have been discovered [*Pushcharovsky et al.,* 2002]. The thin Fe–Mn oxide films developed on the surface of rocks exposed in this basin have elevated Cu and Zn contents [*Bazilevskaya and Skolotnev,* 2002]. A second potentially sulfide-bearing locality is associated with a rift-related basin situated at 5°46′ N, immediately south of the Markov Basin. In the samples from bottom sediments from this basin, A. G. Mochalov established copper sulfides and hydroxides, while Fe–Mn oxide films yielded elevated Ni contents [*Bazilevskaya and Skolotnev,* 2002]. A third locality is a narrow wedge-like rift-related basin, situated north of the Markov Basin and separated from the latter by the Sierra Leone FZ. This locality yielded numerous rock samples with disseminated sulfide mineralization and sulfide veinlets [*Mazarovich et al.,* 2001a; *Peyve et al.,* 2001; *Pushcharovsky et al.,* 2002]. During the first half of Cruise 10 of the R/V Akademik Ioffe, the last locality was named the "Ore area" [*Pushcharovsky et al.,* 2002], and so it will be referred to hereinafter.

The above demonstrates the importance of studying basaltic compositions from the Sierra Leone region, because analyzing them provides clues to the nature and composition of the mantle source, partial melting conditions, and processes occurring in magma chambers, which further elucidates the characteristics of geodynamic regime in this particular region. The regularities of spatial distribution of compositionally diverse basalts permit posing and solving issues such as mantle diapirs beneath the ridge axis, mantle heterogeneity, and sub-lithospheric mantle flows.

Table 1. Coordinates of dredging stations that yielded basalts

Station	Lat	Lon
S2230	6.06	−33.32
S2234	6.34	−33.52
S2235	6.55	−33.46
S2238	6.52	−3371
S2239	6.52	−3380
S2244	6.90	−3395
S2246	7.17	−3393
S2247	7.09	−33.99
S2250	7.08	−34.15
I1003	7.05	−34.42
I1005	7.25	−34.59
I1009	7.12	−33.62
I1010	7.04	−33.68
I1011	7.29	−33.98
I1012	7.04	−34.27
I1016	6.62	−34.10
I1019	6.30	−33.72
I1022	6.31	−3350
I1025	6.33	−3360
I1026	6.36	−3353
I1027	6.37	−33.57
I1028	6.27	−33.40
I1029	6.63	−33.15
I1030	6.65	−33.06
I1031	6.00	−33.24
I1032	5.91	−33.18
I1036	5.41	−33.07
I1037	5.38	−32.98
I1039	5.67	−32.94
I1040	5.77	−33.05
I1045	5.04	−32.76
I1046	5.05	−32.88
I1055	5.38	−32.84
I1057	5.61	−33.19
I1060	5.84	−33.23
I1063	5.91	−33.16
I1068	5.91	−33.18
I1069	5.91	−33.16
I1072	6.68	−33.81

The interest in the study of basalts is furthered by the finds of ocean floor sulfide occurrences in this region. By now, along the entire 20,000-km length of the MAR, direct observations (from submersibles, by video recording and near-bottom measurements) have confirmed the existence of a total of ten hydrothermal fields with high-temperature discharge, or the "black smokers." These discoveries and the non-uniformity of distribution of the fields of high-temperature discharge pose the issue of the cause of genesis of hydrothermal mineralizing systems and of how to develop

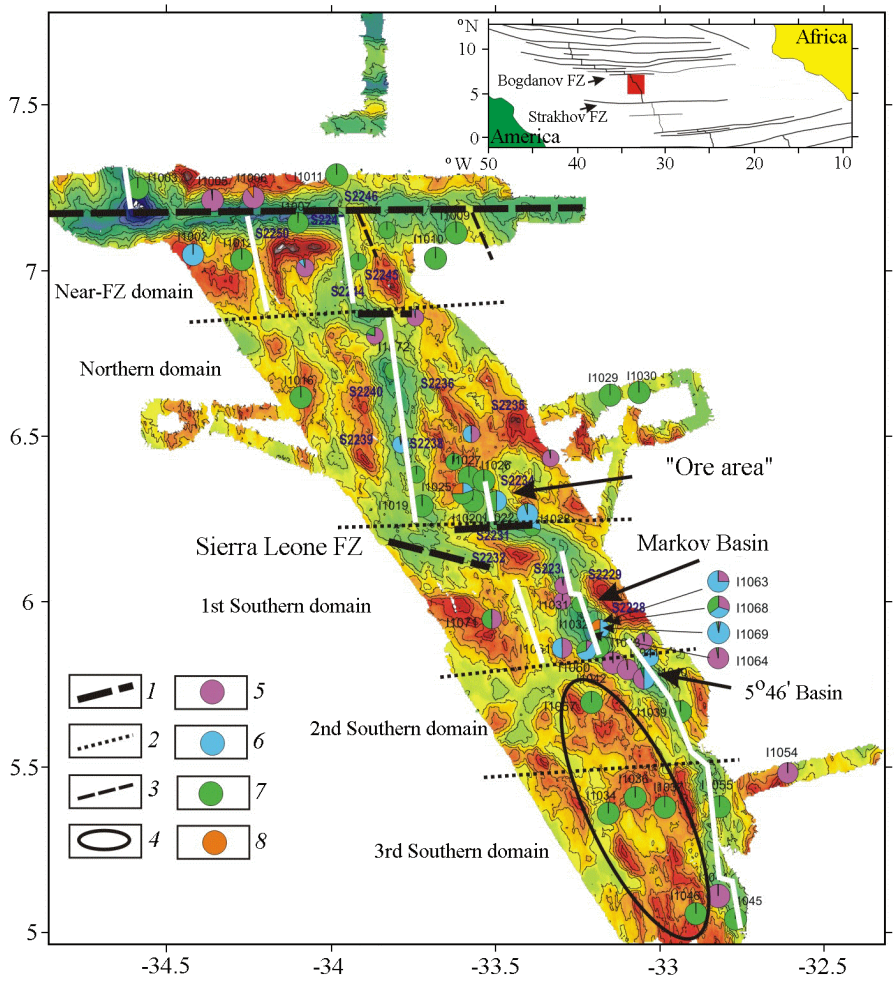

Figure 1. Sketch map showing structural divisions within the Sierra Leone region and location of dredging stations. Symbols: 1 – FZ valley axis, 2 – boundary between various structural domains, 3 – axis of a neovolcanic ridge or its ancient analogue, 4 – outline of the Southwest outcrop domain of basalts, 5 – peridotite, 6 – gabbro, 7 – basalt, 8 – rocks with sulfide mineralization. White line depicts valley axes of active, abandoned, and nascent rifts. Based on data from *Mazarovich et al.* [2001c]. Inset shows the survey area in the framework of the Atlantic floor structure.

guides for their search. The features of volcanism specific to mineralized regions may prove to be a decisive factor to unraveling the nature of the mineral potential and to provide an important exploration criterion.

This issue is so crucial that the costly marine surveys gained support from the Presidium of the Russian Academy of Sciences; their funding was provided under two specialized projects: Geology, Hydrothermal Activity, and Geodynamics of the Sub-equatorial Atlantic (under scientific leadership of Academician Yu. M. Pushcharovsky of the Geological Institute, Russian Academy of Sciences) and Oceanic Mineralizing and Magmatic Systems: Mineral Formation Conditions, Sources of Metals, and Fluids, and the Prospects of Development (under scientific leadership of Dr. N. S. Bortnikov of the Institute of Geology of Ore Deposits, Russian Academy of Sciences).

Principal Features of the Geological Structure and History of the Sierra Leone Region

The northern boundary to our study region is formed by the Bogdanov FZ with an offset of ca. 60 km [*Mazarovich et al.*, 2001b] (Figure 1). In the vicinity of intersection of this FZ with the northern segment of the rift (western intersect), a deep nodal basin is developed, whose slopes are composed of basalts (Station 1003). Location of dredge stations is shown in Figure 1, and coordinates of those stations that yielded basalts are listed in Table 1. In the vicinity of the eastern intersect of the Bogdanov FZ, in place of a nonexistent nodal basin, a large neovolcanic rise made up of young basalts is situated (Station 2246), jutting deeply into

the transform valley from the side of the southern segment of the rift. The Bogdanov FZ has an architecture that is typical of such structures. Along its entire active part on its northern side, there stretches a transverse ridge. It is composed of both basalts (Stations 1005, 1011) and ultramafites alike (Stations 1005, 1006). In the southern part of the FZ, in the vicinity of the eastern intersect, a large corner high is developed, which is elongated in a roughly EW direction. At the base of the corner high, basalts have been encountered (Stations 2247, 1007), and on its upper slope, ultramafites, gabbroids, and dolerites (Station 2250) occur, which is likely to be suggestive of imbricate thrust architecture for this high.

The Sierra Leone region proper, in terms of the ocean floor structure and composition within it, is subdivided into several domains (tectono-magmatic provinces). North of the Sierra Leone FZ, the large Northern domain is situated (Figure 1). Over the entire area of the Northern domain, there stretches a distinctly developed wide and long rectilinear rift valley, modified by minor neovolcanic rises and rift basins as deep as 4500 m. The bottom of the rift valley (Station 2239), the rift basins (Station 1019), and the neovolcanic rises (Stations 2238, 1072) are composed of fresh young basalts. On the western slope of the rift valley, gabbroic rocks are developed. The bathymetry of the western flank of the crestal zone in the vicinity of the Northern domain displays multiple ridges. These are parallel to the rift valley and trend ca. 350°. On the western flank of the crestal zone, Station 1016 yielded basalts. On the opposite, eastern flank the topographic relief is chaotic due to a combination of multiple ridges and large isometric rises, with ridges on the eastern flank being not parallel to the rift valley and trending roughly 335°. This region abounds in ultramafites and gabbroic rocks (Stations 2235, 2236). Some 40 km away of the rift axis, on the eastern flank, the topography also acquires a multiple ridge character, dredge hauls from this region having recovered only basalts (Stations 1029, 1030). These facts suggest that at ca. 2–2.5 Ma (in compliance with the spreading rate for this MAR segment), a change in the geodynamic regime took place in the vicinity of the Northern domain. The magmatic regime typical of the MAR spreading gave way to a regime under which tectonic processes acquired a great role. This regime takes place during the current phase as well.

On the north, the Northern domain bounds on the Near-FZ domain, which adjoins the Bogdanov FZ from the south. The boundary between the two domains is provided by a sinistral strike slip with a ca. 20-km strike separation, running along 6°50′ N. In the axial part of the MAR, the strike slip is expressed by a deep roughly EW trending valley, limited on the west by a small rise, chiefly composed of serpentinized ultramafites with a high degree of hydrothermal reworking and of some basalts (Station 2244). The Near-FZ domain has an asymmetrical structure. The rift valley gives way eastward to a large neovolcanic rise, which, as mentioned above, crosses almost the entire width of the Bogdanov FZ. On the north, this rise gives way to a large isometric rise, whose slopes yielded almost solely ultramafites (Station 2245). Thirty-five kilometers east of the neovolcanic rise, there occurs a similar (in terms of its shape and dimensions) rise, also jutting deeply into the Bogdanov FZ valley. This rise is composed of basalts (Station 1009), which, unlike the basalts from the neovolcanic rise, are altered more strongly and are covered by a Fe–Mn oxide crust. Therefore, the totality of evidence suggests that this rise is a likely ancient analogue to the neovolcanic rise. The topography between the two neovolcanic rises is characterized by multiple small ridges. Dredge hauls from this domain recovered basalts (Station 1010). To the west, 35 km away from the rift, there occurs a roughly NS trending depression resembling the rift valley in terms of its shape and dimensions and with thin sedimentary cover. The western slope of this depression yielded basalts (Station 1012). This feature might be an abandoned rift. This depression separates the corner high mentioned above from the southern transverse ridge of the Bogdanov FZ. The corner high occurs in structural ensemble with the two roughly NS trending ridges that stretch southward from the high.

The Sierra Leone FZ separates the Northern domain from the more southerly regions. The fracture is of a non-transform nature, and it is a sinistral strike slip. Along it, the main axis of the rift valley, marked by the greatest depths, stretches for some 35 km. The Sierra Leone FZ is structurally complex, and it is as wide as 25 km. It consists of two nearly parallel, roughly EW trending topographic lows separated by a major rise running roughly along the center of the FZ, trending generally N 290° W, and composed of ultramafites (Stations 2231, 2232). These topographic lows near the rift valleys are represented by deep valleys. The northern one, trending roughly EW, merges with the southern branch of the rift via a large valley trending ca. N 290° W. At its western terminus, this fracture valley occurs in continuity with a short wedge-like deep valley parallel to the rift, which is discordant to the dominant structural grain in this part of the crestal zone (trending ca. N 335° W). Taken together, these observations imply that this wedge-like valley is a propagating rift. Sea floor in the propagating rift was surveyed in detail during the first half of Cruise 10 of the R/V Akademik Ioffe (the "Ore area"), to yield the first finds of rocks with disseminated sulfide mineralization from this particular region. The "Ore area" (Stations 2234, 1020–1028) abounds in basalts and gabbroic rocks, the latter ranging in composition from troctolite to isotropic gabbro.

The southern valley of the Sierra Leone FZ trends ca. N 290° W, and on the south it occurs in continuity with a large, more shallow water depression, lacking sedimentary cover and with a finely dissected topography. This depression is parallel to the main axis of the rift system at this segment of the MAR, and it might be a nascent rift.

The area south of the Sierra Leone FZ is subdivided into three tectono-magmatic provinces (domains). The 1st Southern domain, immediately adjacent to the Sierra Leone FZ, accommodates the deepest (up to 5000 m) rift basin, the Markov Basin, from whose eastern slope massive sulfide fragments have been recovered (Station 1032). The eastern slope of this basin is dominated by gabbroic rocks (Stations 1032, 1063, 1068, 1069) with subordinate ultramafites, minor basalts, and sporadic plagiogranites. The gabbroic rocks range in composition from troctolite to isotropic gabbro, often showing a considerable degree of cataclasis and myloni-

tization. On the western slope of the basin, basalts are more widespread (Stations 1043, 1060). The features rimming the Markov Basin are composed of plutonic rocks alone (gabbroic rocks and ultramafites) (Stations 2228, 2229, 1061). The Markov Basin is filled by sedimentary cover up to 40 m thick, its general trend (ca. 335°) departing from the general strike of the rift at this portion of the MAR.

The rift valley within the 1st Southern domain outside the Markov Basin is composed of basalts (Stations 2230, 1031). The features rimming the Markov Basin on its western flank are separated by the mentioned nascent rift from a major rise, whose trend swings from roughly NS on the south to roughly EW on the north, and which is composed of plutonic rocks (Station 1071).

In the southern part of next domain to the south (the 2nd Southern domain), the rift valley trends ca. N 340° W, to acquire a trend that is most typical of this particular MAR segment, 355°, in the northern part of the domain. On the north of the 2nd Southern domain, within the rift zone, a deep (up to 4900 m) rift basin is developed at 5°46′, trending generally ca. N 335° W. Its architecture is similar to that of the Markov Basin. Its bottom is covered by sediments as thick as 40 m, and the slopes are dominated by gabbroic rocks and ultramafites with minor basalts (Stations 1040, 1041). Here, as mentioned above, evidence of mineralizing hydrothermal activity has been recorded as well. The rift zones of the 1st and 2nd Southern domains are offset relative to one another in a sinistral en echelon arrangement. The strike slip zone is on the site of a rise composed of ultramafites only (Station 1042). Closer to the eastern slope, in the rift valley of the 2nd Southern domain, a large neovolcanic rise composed of fresh basalts (Station 1039) is developed.

On the western flank of the 2nd Southern domain, isometric and elongated rises occur trending parallel to the rift valley at this segment (ca. 340°) and to the dominant trend of the rift valley within this particular MAR segment (355°). This is also the locus of a system of large interconnected depressions with sediment fill. Some of the depressions are parallel to the rift valley, and they might be abandoned rifts. Judging from the structure of sedimentary cover, in and around these depressions vertical block uplifts of the ocean floor take place. The western flank of the 2nd Southern domain has yielded only basalts (Station 1057).

The 3rd Southern domain has a rectilinear, distinctly developed rift valley, modified by several relatively small neovolcanic rises composed of basalts (Stations 1045, 1055). One of the localities on the western slope of the rift valley is composed of ultramafites (Station 1044). The western flank of the crestal zone in this locality has a topography characterized by multiple ridges. Most ridges are rift parallel, although some rises run parallel to the rift trend within the 2nd Southern domain. On the western flank of the crestal zone of this domain, dredge hauls from several stations recovered only basalts (1034, 1036, 1037, 1046). Therefore, the southwest corner of the surveyed Sierra Leone region displays the large Southwestern outcrop area of basalts (including Station 1057). Note that the region of the Southwestern area is the most uplifted seafloor tract within the Sierra Leone region under study.

On the eastern flank of the crestal zone, the topography, judging from the fragmentary seafloor bathymetry surveys in this region, has a chaotic pattern. One structure on the eastern flank yielded ultramafites (Station 1054).

To summarize our description of the geological structure of the Sierra Leone region, four unique features of this region should be emphasized. These are (1) the broad development of plutonic rocks in the axial spreading zone along the entire length of the region, (2) the presence of several non-transform sinistral strike slips, (3) the broad development of NW trending features oblique to the general strike of the rift, and (4) the ubiquitous asymmetry in the structure of the eastern and western flanks of the crestal zone. These and the other unique geological features of this region are due to its transitional character, which was discussed early in this paper. These features suggest that the MAR segment situated north of the Bogdanov FZ undergoes a sinistral en echelon offset relative to the near-equatorial segment of the MAR. Between the two segments that are being offset, a singular pull apart system is coming into existence, in which transtension related processes are being superimposed over spreading related ones. In the rear (eastern) part of the strike slip, high permeability conditions are created, the result being that large protrusions of serpentinized ultramafites develop there. Apparently, it is for this reason that neovolcanic rises are also confined mainly to the eastern part of the rift zone. Serpentinized ultramafite protrusions are also formed in the rift valley, in the zone of strike slips proper. The deepest rift basins (Markov and the 5°46′) came into being in those localities where the tensile component of the stress field coincided with lithospheric extension due to seafloor spreading. As a result, the basin floor subsides, growing around the basinal periphery and accumulating sediments, whereas on the basin slopes plutonic rocks are being exhumed along the planes of deep detachments initiated by NW trending faults. The fact that the basin slopes display abundant gabbroic rocks constituting a highly evolved suite (to plagiogranite inclusive) and the extreme paucity of fresh basalts suggest that beneath these basins magmatism is chiefly implemented in the form of plutonism. Most likely, under these rift basins long lived magma chambers are in operation. A similar geologic setup is observed in the vicinity of the "Ore area." The wedge-like depression, whose slopes show widespread gabbroic rocks that also comprise a highly evolved suite, is filled with sediments. Apparently, beneath this depression one may expect the presence of a long lived magma chamber as well.

As discussed above, the singular geodynamic regime of spreading, under which the role of tectonic processes increased, was in all likelihood established at 2–2.5 Ma. Apparently, thenceforth, the study region has been under the impact of transtensional stresses. Note also that magmatic activity in the Sierra Leone region has not been reduced as compared to its neighboring MAR segments. It is only a seeming effect that magmatic activity appears to have ebbed in the environment of a dramatically increased tectonism (due to the combination of seafloor spreading with transtensional movements of a different nature).

Major and Trace Element Characteristics of Basalts and their Chilled Glasses

Major and trace element composition for the basalts under study are listed in Table 2, and those for representative chilled basaltic glasses, in Table 3 (a total of 253 glasses were analyzed). The rare-earth element contents are listed in Table 4.

The most representative basalt population was obtained from rift-related structures of the Northern domain (Stations 2238, 2239, 2240, 1019, 1072). Basalts of this domain are rather uniform in composition and are distinguished by their high MgO content. It is particularly high in basalts from Stations 1019 (8.79–9.51% MgO in basalts and 7.96–8.56% MgO in glasses) and 1072 (8.93–9.30% MgO in basalts and 7.91–8.22% in glasses), characterizing the deepest rift basins of the Northern domain. The MgO contents of these basalts are perceptibly higher than in most basalts that compose the axial MAR zone situated immediately north of the Sierra Leone region near the Arkhangelsky, Doldrums, and Vernadsky FZs [*Pushcharovsky et al.,* 1992]. Equally high MgO contents are characteristic of basalts from certain structures located between the Cape Verde and Marathon FZs [*Skolotnev et al.,* 1999]. It is common knowledge that the MAR segment between the Cape Verde and Marathon FZs is remarkable in its being abundant in enriched basalts [*Dosso et al.,* 1991] and in that it displays active "black smokers," or the Logachev mineralized field [*Bogdanov et al.,* 1997].

Klein and Langmuir [1987] in recalculating compositions of chilled basalt glasses used the value of 8% MgO as a characteristic of initial melt. To use this criterion, most basalts under study are classed as very slightly evolved or virtually non-evolved varieties. Indeed, the most primitive (high-Mg) basalts, e.g., from Station 2238 (8.07–8.96% MgO), have very low potassium (0.08–0.09% K_2O) and phosphorus contents (0.08–0.11% P_2O_5), reduced titanium (1.35% TiO_2), iron (7.94–8.81% FeO^*), and sodium contents (2.52–2.66% Na_2O), elevated calcium (10.61–11.50% CaO) and aluminum contents (15.83–18.05% Al_2O_3), and low FeO*/MgO ratios (0.94–1.08). The lower magnesian basalts from this Station (7.69–8.00% MgO), apparently, are more evolved varieties, inasmuch as they are also distinguished by higher contents of iron oxides (10.35–11.17% FeO^*), titanium (1.51–1.67% TiO_2), potassium (0.16–0.22% K_2O), sodium (2.74–2.87% Na_2O), and phosphorus (0.14–0.16% P_2O_5) and by lower contents of calcium (10.43–10.54% CaO) and aluminum (14.74–15.97% Al_2O_3), their FeO^*/MgO ratio ranging 1.30–1.41.

Despite the overall compositional uniformity of the basalts under study, there are some minor, albeit telling distinctions between them. Basalts from the rift basin located nearer the Sierra Leone FZ (Station 1019) (1.25–1.29% TiO_2, 0.09–0.11% K_2O, 0.10–0.11% P_2O_5), while having similar MgO contents, are distinguished from basalts of the more northerly basin (Station 1072; 1.13–1.15% TiO_2, 0.08–0.09% K_2O, 0.08–0.09% P_2O_5) in having higher contents of titanium, potassium, and phosphorus oxides. Evidently, mantle source compositions or generation conditions for the melts initial to basalts of these two rift-related basins were dissimilar. Station 2238 basalts are more similar to Station 1019 ones, more distant from the former.

Variation patterns for glass compositions are generally close to those for the basalts, although the measured glass chemistries rarely coincide with their host basalt ones, having as a rule higher titanium and sodium contents and lower magnesium abundances.

The basalts in point are characterized by very low incompatible element abundances. The most primitive varieties have 1.8–2.9 ppm Nb, 73–75 ppm Zr, and 23–24 ppm Y. The more evolved varieties have as much as 3.8 ppm Nb, 120 ppm Zr, 35 ppm Y, and 1.4 ppm Rb. The $(Nb/Zr)_n$ ratios in rift-related basalts from the Northern domain are also very low, equaling 0.27–0.38, which places these basalts with derivatives of an N-MORB-like tholeiitic melt [*Sun et al.,* 1979]. This conclusion is further supported by the character of their rare-earth element (REE) spectrum and the low K/Ti ratio (0.09–0.45) for their chilled glasses. The REE spectrum plots at 10–20 times the chondritic level and has a characteristic low in the light lanthanide region ($(La/Sm)_n$ = 0.57–0.62) (Figure 2a). Analysis of these spectra implies that even the high-Mg basalts are evolved, because they have slight negative Eu anomaly (Smp. 2239/1). The less magnesian samples have more marked negative Eu anomaly (Smp. 2238/3).

Basalts from the western flank of the crestal zone of the Northern domain (Station 1016), just like the rift basalts, are high-Mg, although at the same Mg content they are considerably higher in titanium (1.55–1.61% TiO_2), potassium (0.11–0.26% K_2O), phosphorus (0.14–0.18% P_2O_5), and sodium (2.75–2.82% Na_2O) and lower in alumina (14.81–15.40% Al_2O_3). The measured glass compositions are distinguished in the same manner from the glass compositions from the above stations, although they also differ compositionally from those basalts whose surface they were collected in that they are lower in titanium (1.46–1.54% TiO_2) and magnesium (8.38–8.55% MgO).

Incompatible element abundances of high-Mg basalt varieties from the western flank are a little higher than in the rift-related basalts (5 ppm Nb, 96 ppm Zr, 30 ppm Y, 1.4–2.4 ppm Rb), the $(Nb/Zr)_n$ ratios in the basalts (0.42) and the K/Ti ratios in the glasses (0.42–0.60) also being higher.

Generally, basalts from the eastern flank of the Northern domain are considerably less magnesian. In comparison to the less magnesian basalts from Station 2238, which were discussed above, one should note their similarity and, on the other hand, a minor distinction. The flank basalts are considerably higher in CaO (11.32–11.42%) but somewhat lower in TiO_2 (1.42–1.44%) and P_2O_5 (0.12–0.17%) and higher in K_2O (0.15–0.30%). The collection of basalts from the eastern flank contains a single high-Mg sample (1030/1), similar to basalts from Station 1016, located on the western flank.

In comparison to rift basalts, the high-Mg basalts from the eastern flank are higher in incompatible elements (3.7–4.2 ppm Nb, 97–110 ppm Zr, 29–31 ppm Y, 2.1 ppm Rb) and have a higher $(Nb/Zr)_n$ ratio (0.57), their glasses having K/Ti ratios of 0.47–0.52; they are also high in Cr (420 ppm), Ni (190 ppm), and V (330–350 ppm). The most potassic sample from this group of basalts (Smp. 1029/1) is high in Rb (7.6 ppm), its $(Nb/Zr)_n$ ratio being as high as 0.64,

Table 2. Major- (wt%) and trace-element (ppm) composition of basalts from the Sierra Leone region

Sample	SiO_2	TiO_2	Al_2O_3	Fe_2O_3	FeO	MnO	MgO	CaO	Na_2O	K_2O	P_2O_5	LOI	Total	FeO*	FeO/MgO	Nb	Zr	Y	Rb	Sr	Ba	V	Ni	Cr	$(Nb/Zr)_n$
Bogdanov Fz																									
I1003/1	49.02	1.34	15.62	3.59	5.96	0.15	7.73	11.1	3.43	0.32	0.18	1.15	99.59	9.19	1.19	7.9	100	25	4.8	260	13	250	150	290	0.87
I1003/2	49.3	1.58	15.69	2.32	6.78	0.17	8.17	10.95	3.18	0.08	0.14	1.2	99.56	8.87	1.09										
I1003/4	49.23	1.46	15.88	2.51	6.95	0.16	7.1	11.07	3.3	0.39	0.18	1.24	99.47	9.21	1.30										
I1003/6	48.29	1.46	16.15	3.49	6.12	0.17	7.71	10.94	3.54	0.33	0.18	1.26	99.64	9.26	1.20										
I1003/7	48.51	1.47	16.16	4.27	5.6	0.16	7.63	10.8	3.5	0.3	0.18	1.36	99.94	9.44	1.24										
I1005/1	48.5	1.68	15.66	2.5	6.64	0.15	9	10.31	3.31	0.17	0.2	1.6	99.72	8.89	0.99	5.7	130	28	1.2	190	14	340	200	330	0.48
I1005/39	47.58	1.11	15.94	2	7.73	0.18	10.01	11.13	2.39	0.11	0.08	1.35	99.61	9.53	0.95	1.7	59	22	2	120	7	200	210	400	0.32
I1011/1	46.89	1.81	15.38	4.39	6.49	0.19	7.62	11.04	2.98	0.2	0.19	2.15	99.33	10.44	1.37	3.3	120	36	1.1	130	5	330	140	290	0.30
Near-FZ domain																									
S2244/50	50.14	1.71	14.19	3.51	7.15	0.18	8.78	10.67	2.69	0.16	0.15	0.43	99.76	10.309	1.17	4.9	100	30	2.3	120	47				0.54
S2244/51	51.3	1.54	14.76	2.23	7.21	0.17	8.66	10.81	2.62	0.15	0.13	0.46	100.04	9.217	1.06										
S2244/55	50.66	1.78	13.96	1.99	8.05	0.17	8.64	10.51	2.73	0.16	0.16	0.93	99.74	9.841	1.14	5.3	110	33	2.1	110	55				0.53
S2244/61	50.78	1.52	14.94	1.86	7.43	0.18	8.57	10.89	2.67	0.13	0.13	0.71	99.81	9.104	1.06	3.3	91	30	1.9	120	16				0.40
S2244/62	50.04	1.5	15.52	3.38	7.22	0.15	8.62	10.81	2.58	0.15	0.12	0.64	100.73	10.262	1.19	3.1	86	26	1.5	120					0.40
S2244/64	49.39	1.13	16.44	2.73	5.58	0.15	8.04	11.75	2.29	0.14	0.08	1.88	99.6	8.037	1.00										
S2246/1	50.2	1.76	14.66	1.95	7.82	0.18	8.23	10.42	3.03	0.16	0.15	1.03	99.59	9.575	1.16	3.6	110	31	2.1	140	30				0.36
S2246/2	49.66	1.74	14.64	3.44	8.14	0.18	7.74	10.04	3	0.15	0.16	0.64	99.53	11.236	1.45	3.8	110	34	1.6	140	18				0.38
S2246/5	49.42	1.78	15.29	5.2	6.08	0.18	8.69	10.02	3.09	0.15	0.16	0.1	100.16	10.76	1.24	3.8	110	33	1.6	140	33				0.38
S2246/7	49.52	1.76	15.13	5.15	6.16	0.18	8.69	10.02	3.08	0.16	0.16	0.1	100.11	10.795	1.24	3.4	110	33	1.4	140	42				0.34
S2247/4	49.28	1.76	15.2	5	6.35	0.19	8.75	9.97	3.04	0.16	0.15	0.1	99.95	10.85	1.24	3.5	110	31	1.7	140	5				0.35
S2250/56	47.1	1.63	15.54	3.71	5.68	0.22	10.3	10.64	2.49	0.09	0.13	2.34	99.87	9.019	0.88	3	92	29	1	110	21				0.36
I1009/1	49	1.22	15.67	3.55	5.49	0.15	8.24	12.04	2.8	0.15	0.1	1.47	99.88	8.69	1.05	1.5	63	23	2.7	110	8	270	140	330	0.26
I1010/1	49.2	0.97	15.65	3.55	5.4	0.15	9.07	11.57	2.51	0.1	0.08	1.89	100.14	8.60	0.95	1.7	55	21	1.3	130	5	220	220	420	0.34
I1010/2	46.58	1.01	17.22	4.02	5.73	0.16	9.18	11.89	2.51	0.07	0.12	1.18	99.67	9.35	1.02										
I1012/1	49.67	1.45	15.81	1.62	7.83	0.18	8.86	10.68	2.84	0.13	0.16	1.01	100.24	9.29	1.05	4.2	94	27	1.7	120	6	300	170	360	0.49
I1012/2	49.19	1.54	15.18	1.35	7.76	0.17	8.85	11.15	2.78	0.13	0.15	1.16	99.41	8.98	1.01										
I1012/3	50.26	1.43	15.5	0.82	7.94	0.17	8.76	10.81	2.75	0.11	0.14	0.84	99.53	8.68	0.99										
Northern domain																									
S2235/5	49.45	1.39	14.87	3.75	7.54	0.2	8.22	10.96	2.45	0.07	0.16	0.9	99.96	10.915	1.33	3.5	60	29	1.5	110	33				0.64
S2238/10	50.47	1.42	15	3.05	6.75	0.18	7.92	10.54	2.83	0.14	0.11	1.25	99.66	9.495	1.20	3	92	28		110	34				0.36
S2238/3	49.06	1.67	14.74	3.16	8.33	0.22	7.92	10.43	2.78	0.21	0.16	0.72	99.4	11.174	1.41	3.8	120	35		110	35				0.35
S2238/7	49.62	1.51	15.14	2.84	7.83	0.19	8	10.54	2.87	0.22	0.14	0.67	99.57	10.386	1.30	3.8	110	31	1.7	120	40				0.38
S2238/25	48.7	1.09	18.05	1.81	6.79	0.14	8.96	11.46	2.59	0.11	0.06	0.23	99.99	8.419	0.94										
S2238/26	49.56	1.61	15.97	2.89	7.75	0.22	7.69	10.47	2.74	0.16	0.15	1.09	100.3	10.351	1.35	3.5	100	31	1.4	120	59				0.39
S2239/1	50.42	1.35	16.83	1.01	7.46	0.16	8.48	11.38	2.57	0.09	0.09	0.11	99.95	8.369	0.99	1.8	73	23		120	33				0.27
S2239/2	49.88	1.35	16.75	1.44	7.26	0.16	8.07	11.36	2.52	0.09	0.1	0.77	99.75	8.556	1.06	2.3	75	24		110	18				0.34

Table 2. Continued

Sample	SiO_2	TiO_2	Al_2O_3	Fe_2O_3	FeO	MnO	MgO	CaO	Na_2O	K_2O	P_2O_5	LOI	Total	FeO^*	FeO/MgO	Nb	Zr	Y	Rb	Sr	Ba	V	Ni	Cr	$(Nb/Zr)_n$
Northern domain																									
S2239/3	50.35	1.36	16.51	2.02	7.13	0.16	8.28	11.38	2.6	0.09	0.09	0.35	100.32	8.948	1.08	2.9	74	24		120	37				0.43
S2239/5	50.56	1.33	16.23	2.19	5.97	0.14	8.32	11.5	2.66	0.1	0.1	0.75	99.85	7.941	0.95	2.4	73	24		120	70				0.36
I1016/2	48.96	1.58	14.81	3.04	7.16	0.18	8.96	10.94	2.76	0.15	0.16	1.16	99.86	9.90	1.10	5	96	30	2.1	130	9	310	210	380	0.57
I1016/3	49.23	1.55	15.03	2.37	6.76	0.17	8.93	10.7	2.75	0.26	0.14	1.6	99.49	8.89	1.00										
I1016/4	47.88	1.56	15.4	2.78	6.58	0.18	9.53	11.06	2.82	0.18	0.15	1.28	99.4	9.08	0.95										
I1016/8	48.57	1.61	15.24	2.74	7.04	0.19	8.89	11.23	2.76	0.11	0.18	1.2	99.76	9.51	1.07										
I1019/3	50.37	1.26	15.07	2.5	7.41	0.16	8.79	11.51	2.61	0.11	0.11	0.42	100.36	9.66	1.10	3.4	77	24	1	120	9	280	190	360	0.49
I1019/12	50.24	1.3	16.2	0.93	7.57	0.16	9.06	11.43	2.61	0.1	0.1	0.16	99.82	8.41	0.93										
I1019/34	49.71	1.28	16.09	1.3	7.38	0.12	9.23	11.46	2.63	0.09	0.1	0.5	99.89	8.55	0.93	3	71	24	1	120	11	280	190	380	0.46
I1019/37	48.87	1.25	15.87	1.87	6.78	0.16	9.51	11.14	2.5	0.09	0.11	1.25	99.4	8.46	0.89										
I1019/40	49.52	1.29	15.75	1.85	6.85	0.17	9.35	11.58	2.55	0.09	0.11	0.6	99.71	8.52	0.91										
I1019/44	49.62	1.29	16.27	1.34	7.26	0.17	8.92	11.72	2.62	0.11	0.1	0.47	99.89	8.47	0.95										
I1019/49	49.71	1.28	15.87	2.15	7.12	0.15	9.31	11.32	2.63	0.1	0.1	0.45	100.19	9.06	0.97										
I1029/1	49.61	1.44	15.26	5.51	4.16	0.12	7.5	11.32	2.88	0.3	0.14	1.52	99.76	9.12	1.22	4.7	81	27	7.6	130	14	280	84	330	0.64
I1029/2	49.57	1.42	15.06	4.8	4.77	0.18	7.44	11.42	2.94	0.29	0.13	1.8	99.82	9.09	1.22										
I1029/3	49.64	1.43	14.68	5.41	5.03	0.15	7.7	11.38	2.61	0.26	0.12	1.78	100.19	9.90	1.29										
I1030/1a	47.6	1.56	16.42	4.67	4.89	0.12	8.75	11.02	2.76	0.15	0.17	1.67	99.78	9.09	1.04	3.7	97	29	1.4	160	12	330	190	420	0.42
I1072/1	48.49	1.06	15.86	3.69	7.28	0.17	8.93	11.5	2.55	0.09	0.09	0.37	100.08	10.60	1.19	3	62	24	<1	110	6	240	170	360	0.53
I1072/3	49.62	1.13	16.17	3.22	5.96	0.16	9.1	10.95	2.55	0.09	0.09	0.53	99.57	8.86	0.97	3.1	62	21	1.3	110	6	230	160	360	0.55
I1072/4	49.15	1.13	16.05	3.24	6.55	0.16	9.3	11.22	2.5	0.08	0.09	0.33	99.8	9.47	1.02	2.6	62	21	1.3	120	7	260	160	340	0.46
I1072/8	49.57	1.15	16.43	2.67	6.51	0.15	9.21	11.11	2.52	0.08	0.08	0.3	99.78	8.91	0.97	2.6	63	22	1.4	110	6	280	180	380	0.45
I1072/11	49.63	1.13	15.95	3.33	6.49	0.15	9.09	10.98	2.5	0.08	0.08	0.46	99.87	9.49	1.04	2.6	63	22	1.6	110	7	270	160	360	0.45
I1072/16	49.4	1.13	16.21	3.37	6.06	0.15	9.09	11.18	2.5	0.08	0.08	0.61	99.86	9.09	1.00	3.4	62	22	1.4	110	5	240	170	350	0.60
"Ore area"																									
S2234/23	49.92	1.33	15.83	3.02	5.72	0.09	8.04	10.68	3.02	0.05	0.08	1.64	99.42	8.438	1.05										
S2234/37	49.16	0.8	17.1	1.06	5.82	0.16	10.24	11.08	2.04	0.04	0.06	1.98	99.54	6.774	0.66	2	52	17		110	21				0.42
I1022/5	50.22	2.11	14.55	2.8	9.24	0.2	6.24	10.05	2.85	0.17	0.19	0.88	99.5	11.76	1.88										
I1022/6	49.94	1.8	15.73	1.81	7.82	0.19	7.7	10.72	2.81	0.24	0.18	1.2	100.14	9.45	1.23										
I1025/1	49.17	1.91	14.7	4.55	7.4	0.16	6.45	10.29	3.03	0.37	0.16	1.94	100.13	11.50	1.78	4.1	110	38	4.8	110	16	350	78	180	0.41
I1025/2	48.83	1.71	15.11	4.46	6.46	0.15	7.52	10.17	2.93	0.32	0.17	1.98	99.81	10.47	1.39										
I1025/4	49.24	1.96	14.05	5.22	7.97	0.19	7	10.14	2.95	0.17	0.16	1.06	100.11	12.67	1.81										
I1025 /8	49.16	1.88	14.21	4.38	8.54	0.18	6.81	10.26	3.1	0.16	0.16	0.83	99.67	12.48	1.83										
I1026/1	50.16	1.55	15.32	4.32	5.26	0.13	7.86	10.88	2.95	0.2	0.14	1.15	99.92	9.15	1.16	4.6	96	30	2.6	130	8	270	96	290	0.53
I1026/2	49.66	1.54	15.93	4.04	5.54	0.08	7.17	10.92	2.94	0.29	0.14	1.5	99.75	9.18	1.28										
I1026/8	49.65	1.49	15.54	4.52	6.07	0.16	7.27	10.54	2.77	0.29	0.14	1.39	99.83	10.14	1.39										
I1026/10	50.15	1.57	16.55	2.15	6.59	0.16	7.69	10.43	2.84	0.35	0.14	1.29	99.91	8.53	1.11										
I1026/20	49.84	1.62	14.17	4.41	7.12	0.09	7.89	9.88	2.86	0.14	0.13	1.76	99.91	11.09	1.41	4.2	97	34	1.7	110	6	310	120	220	0.48

Table 2. Continued

Sample	SiO_2	TiO_2	Al_2O_3	Fe_2O_3	FeO	MnO	MgO	CaO	Na_2O	K_2O	P_2O_5	LOI	Total	FeO*	FeO/MgO	Nb	Zr	Y	Rb	Sr	Ba	V	Ni	Cr	$(Nb/Zr)_n$
"Ore area"																									
I1026/21	49.38	1.69	14.99	4.22	5.29	0.08	8.86	10.28	2.91	0.33	0.19	1.39	99.61	9.09	1.03										
I1026/24	49.96	1.85	14.17	4.86	6.83	0.19	7.36	9.42	3.02	0.38	0.17	1.45	99.66	11.20	1.52										
I1026/25	49.81	1.62	14.63	4.43	6.03	0.18	8.91	9.81	2.9	0.21	0.16	1.13	99.82	10.02	1.12										
I1026/30	49.85	1.37	14.75	4.31	5.09	0.17	9.16	10.49	2.71	0.19	0.11	1.38	99.58	8.97	0.98										
I1027/1	50.51	1.69	14.13	2.55	8.17	0.14	7.77	10.02	2.86	0.19	0.16	1.22	99.41	10.47	1.35	4.4	110	34	2.5	120	15	320	130	240	0.44
I1027/2	50.58	1.47	14.23	4.1	5.54	0.08	8.63	10.89	2.92	0.25	0.15	1.32	100.16	9.23	1.07										
I1027/3	50.2	1.87	13.66	4.73	7.39	0.05	6.99	10.32	2.98	0.26	0.18	1.64	100.27	11.65	1.67										
I1027/4	50.32	1.46	13.82	3.7	7.2	0.17	8.88	10.63	2.69	0.12	0.14	0.86	99.99	10.53	1.19										
I1027/5	50.67	1.75	14.65	3.3	7.08	0.1	6.92	9.59	2.92	0.46	0.17	1.77	99.38	10.05	1.45										
I1027/7	50.61	1.7	14.7	1.26	8.8	0.18	8.1	10.11	2.91	0.16	0.17	0.9	99.6	9.93	1.23										
I1028/18	50.38	1.39	14.09	5.92	5.18	0.15	8.8	10.87	2.72	0.11	0.11	0.47	100.19	10.51	1.19	3.3	80	28	1.6	110	14	290	200	350	0.45
1st Southern domain																									
S2230/1	50.69	1.86	14.88	3.13	8.11	0.18	6.92	10.04	2.9	0.22	0.16	0.37	99.46	10.927	1.58	5.2	110	36	2	110	76				0.52
S2230/2	50.48	1.87	15.22	3.97	6.75	0.18	6.93	10.17	3.01	0.17	0.18	0.63	99.56	10.323	1.49	5.1	120	34	4.2	110	37				0.47
S2230/3	50.37	1.9	14.92	2.91	8.23	0.18	7.02	10.02	2.93	0.24	0.17	0.63	99.52	10.849	1.55	4.9	110	37	4	110	33				0.49
S2230/6	50.25	1.85	15.79	2.23	8.44	0.19	7.19	9.89	2.97	0.23	0.16	0.91	100.1	10.447	1.45										
S2230/10	50.58	1.87	14.32	3.98	7.95	0.2	7.1	10.14	2.88	0.15	0.16	0.51	99.84	11.532	1.62										
I1031/1	50.54	1.54	14.32	4.12	6.73	0.15	7.9	10.54	2.88	0.14	0.16	0.87	99.89	10.44	1.32	3.7	88	30	1.6	110	12	300	110	220	0.46
I1031/2	50.2	1.52	14.94	2.76	7.5	0.16	8.4	10.18	2.84	0.13	0.14	0.93	99.7	9.98	1.19										
I1031/3	50.95	1.82	14.75	3.34	7.71	0.11	6.96	9.88	3.02	0.16	0.17	1.16	100.03	10.72	1.54										
Markov Basin																									
I1032/22	50.19	1.38	14.47	5.88	4.73	0.11	8.2	10.33	2.98	0.16	0.13	1.46	100.02	10.02	1.22	4.8	93	32	2.5	160	13	300	180	220	0.57
I1032/23	49.81	1.67	14.96	4.88	5.94	0.14	8.33	9.86	2.93	0.24	0.13	1.26	100.15	10.33	1.24										
I1032/24	50.57	1.7	14.55	5.01	5.28	0.13	6.72	11.09	2.87	0.26	0.18	0.78	99.14	9.79	1.46										
I1032/27	49.92	1.69	15.04	3.75	6.86	0.11	7.6	10.73	2.82	0.26	0.15	1.29	100.22	10.24	1.35										
I1032/29	48.48	1.66	15.42	6.27	4.82	0.16	8.6	10.39	3.08	0.17	0.16	0.68	99.89	10.46	1.22										
I1032/40	50.46	1.68	15.41	3.99	6.13	0.15	7.25	10.56	2.73	0.35	0.15	0.8	99.66	9.72	1.34	6.9	97	34	5.1	120	11	280	100	260	0.78
I1032/42	50.4	1.62	14.94	3.83	6.66	0.13	7.6	10.57	2.89	0.26	0.17	0.87	99.94	10.11	1.33										
I1040/2	49.82	1.54	14.92	3.43	6.18	0.2	8.1	10.63	2.87	0.39	0.17	1.23	99.48	9.27	1.14										
I1040/3	49.18	1.2	15.34	3.72	5.57	0.15	9.13	10.81	2.63	0.14	0.11	1.52	99.5	8.92	0.98										
I1060/1	48.96	1.23	15.86	2.28	6.64	0.12	9.42	10.69	2.49	0.06	0.1	1.77	99.62	8.69	0.92	4.6	72	23	<1	110	<5	260	180	340	0.70
I1060/2	50.19	1.05	15.37	1.49	7.04	0.17	8.91	11.08	2.75	0.12	0.1	1.72	99.99	8.38	0.94	4.6	80	32	<1	90	7	270	100	280	0.63
I1060/3	49.6	0.93	16.27	1.52	5.95	0.15	9.53	11.74	2.41	0.11	0.06	1.15	99.42	7.32	0.77	3.7	48	17	1.3	96	12	220	140	550	0.85
I1060/7	48.69	1.05	16.78	1.59	7.17	0.18	10.2	10.86	2.44	0.13	0.07	0.7	99.86	8.60	0.84	2.7	64	22	1.5	110	<5	220	200	390	0.46
I1060/8	49	1.05	16.52	2.26	7.43	0.17	9.47	10.52	2.41	0.08	0.07	0.61	99.59	9.46	1.00	2.9	61	22	<1	110	86	200	200	390	0.52
I1060/I106	50.8	1.26	15.3	0.94	8.05	0.19	8.5	11.49	2.73	0.14	0.09	0.67	100.16	8.90	1.05										
I1063/23	49.27	1.09	16.04	1.03	7.44	0.15	9.23	11.24	2.72	0.09	0.17	1.22	99.69	8.37	0.91	3.5	32	23	<1	100	6	220	170	390	1.20

Table 2. Continued

Sample	SiO_2	TiO_2	Al_2O_3	Fe_2O_3	FeO	MnO	MgO	CaO	Na_2O	K_2O	P_2O_5	LOI	Total	FeO*	FeO/MgO	Nb	Zr	Y	Rb	Sr	Ba	V	Ni	Cr	$(Nb/Zr)_n$
Markov Basin																									
I1068/1	50.4	1.91	15.47	1.07	8.43	0.14	7.3	9.72	2.99	0.27	0.18	1.37	99.25	9.39	1.29	5.5	120	37	2.1	110	32	330	100	180	0.50
I1068/2	49.9	1.66	15.97	1.94	6.8	0.15	7.69	11.05	2.78	0.18	0.15	1.52	99.79	8.55	1.11	6.2	96	30	3.5	120	8	310	120	290	0.71
I1068/3	49.88	1.71	15.83	2.59	6.52	0.13	7.73	10.47	2.83	0.3	0.15	1.48	99.62	8.85	1.15	6.5	97	30	3.8	130	8	320	130	300	0.74
I1068/4	50.1	1.63	14.54	3.54	7.16	0.17	7.36	11.18	2.74	0.27	0.14	0.69	99.52	10.35	1.41	6.4	98	30	2.8	120	7	340	120	310	0.72
I1068/5	49.65	1.67	14.43	3	7.35	0.2	7.81	11.07	2.71	0.27	0.16	1.2	99.52	10.05	1.29	7.7	100	32	3.7	140	8	330	83	250	0.85
I1068/6	49.57	1.62	13.93	2.99	7.51	0.06	8.32	10.22	2.84	0.31	0.13	1.94	99.44	10.20	1.23	5.4	99	32	4.5	120	7	310	140	230	0.60
I1068/7	49.67	1.65	15.22	2.72	6.28	0.13	7.92	10.72	2.93	0.2	0.15	1.76	99.35	8.73	1.10	7.2	100	31	2.9	130	28	320	120	260	0.79
I1068/15	49.46	1.65	15.16	2.37	8.17	0.19	8.11	10.7	2.69	0.32	0.16	0.99	99.97	10.30	1.27	7.6	100	32	4	130	52	320	130	260	0.84
I1068/16	49.91	1.58	15.31	1.94	7.68	0.21	7.74	11.19	2.8	0.3	0.16	0.78	99.6	9.43	1.22	6.7	98	30	3	120	34	330	100	310	0.75
I1068/23	49.92	1.01	15.22	3.21	7.07	0.18	8.54	10.96	2.73	0.09	0.08	0.92	99.93	9.96	1.17	3.9	71	25	<1	120	8	270	120	220	0.60
I1069/1	49.75	1.76	14.02	2.8	8.67	0.19	8.13	9.94	2.78	0.31	0.17	0.98	99.5	11.19	1.38	5.3	120	36	2.1	110	28	320	110	240	0.49
2nd Southern domain																									
I1039/1	49.3	1.37	13.89	5.11	6.47	0.17	8.93	10.53	2.93	0.16	0.14	0.72	99.72	11.07	1.24	4.9	89	31	2.2	120	5	330	160	330	0.61
I1039/2	49.38	1.48	14.75	3.51	6.83	0.18	8.32	10.96	2.8	0.14	0.14	0.96	99.45	9.99	1.20										
I1039/3	49.46	1.47	14.18	3.35	7.62	0.17	8.56	10.64	2.77	0.15	0.13	0.85	99.35	10.64	1.24										
I1039/5	48.94	1.49	14.38	2.84	7.72	0.19	8.95	10.94	2.73	0.16	0.13	0.96	99.43	10.28	1.15										
I1039/6	49.1	1.48	14.54	3.35	7.33	0.18	8.97	10.56	2.78	0.17	0.13	0.91	99.5	10.35	1.15										
I1039/7	48.64	1.48	14.9	2.76	7.4	0.18	8.99	10.8	2.77	0.16	0.13	1.12	99.33	9.88	1.10										
I1039/8	49.56	1.44	14.1	4.67	6.29	0.18	8.89	10.81	2.81	0.16	0.15	0.7	99.76	10.49	1.18										
3rd Southern domain																									
I1045/1	49.16	1.33	17.52	2.28	6.02	0.16	7.4	11.45	2.74	0.17	0.11	1.38	99.72	8.07	1.09	3.4	79	24	2.1	140	5	290	120	300	0.47
I1045/2	49.74	1.41	16.1	2.18	7.02	0.17	7.64	10.77	2.73	0.18	0.14	1.21	99.29	8.98	1.18										
I1045/3	49.76	1.29	16.48	1.98	6.68	0.16	8.85	11.13	2.65	0.1	0.1	0.48	99.66	8.46	0.96										
I1045/4	49.19	1.28	17.17	2.62	6.36	0.15	8.19	11.39	2.61	0.15	0.11	0.34	99.56	8.72	1.06										
I1045/5	49.48	1.29	16.62	2.56	7.05	0.15	7.87	11.4	2.5	0.13	0.11	0.61	99.77	9.35	1.19										
I1045/6	49.15	1.32	16.57	2.62	6.79	0.16	7.96	11.44	2.7	0.22	0.11	0.56	99.6	9.15	1.15										
I1045/7	49.1	1.3	16.9	2.67	6.41	0.15	8.5	11.34	2.63	0.21	0.11	0.6	99.92	8.81	1.04										
I1045/11	49.48	1.21	16.11	1.96	7.3	0.16	8.92	11.29	2.54	0.1	0.11	0.6	99.78	9.06	1.02										
I1055/1	48.82	1.77	15.19	2.76	8.66	0.18	7.46	11.21	2.81	0.18	0.15	0.24	99.43	11.14	1.49										
I1055/2	49.87	1.74	14.94	2.57	8.6	0.18	7.1	11.11	2.84	0.2	0.15	0.88	100.18	10.91	1.54										
I1055/3	50.2	1.76	15.25	2.13	8.69	0.18	7.18	10.9	2.85	0.19	0.16	0.6	100.09	10.61	1.48										
I1055/5	50.45	1.7	15.05	2.5	8.48	0.15	7.05	10.83	2.83	0.17	0.17	0.58	99.96	10.73	1.52										
I1055/6	50.17	1.71	14.93	2.74	8.23	0.14	7.38	10.74	2.84	0.17	0.15	0.91	100.11	10.70	1.45										
I1055/8	49.33	1.73	14.88	4.75	6.6	0.16	7.56	10.9	2.84	0.2	0.14	0.79	99.88	10.88	1.44										
I1055/9	49.95	1.74	14.99	2.91	7.86	0.07	7.81	10.61	2.84	0.18	0.15	0.42	99.53	10.48	1.34										
I1055/11	49.28	1.76	14.61	3.28	7.95	0.15	8.32	10.7	2.92	0.18	0.15	0.89	100.19	10.90	1.31										

Table 2. Continued

Sample	SiO_2	TiO_2	Al_2O_3	Fe_2O_3	FeO	MnO	MgO	CaO	Na_2O	K_2O	P_2O_5	LOI	Total	FeO^*	FeO/MgO	Nb	Zr	Y	Rb	Sr	Ba	V	Ni	Cr	$(Nb/Zr)_n$
Southwestern outcrop area																									
I1036/1	47.94	1.68	15.04	6.98	3.38	0.16	7.11	10.81	3.11	0.34	0.2	2.62	99.37	9.66	1.36	14	120	30	6.6	180	91	280	110	250	1.28
I1036/2	49.06	1.54	14.82	5.67	5.39	0.17	7.39	10.64	3.06	0.46	0.17	1.2	99.57	10.49	1.42										
I1036/3	49.68	1.58	15.15	4.79	5.53	0.16	7.03	10.64	2.95	0.5	0.17	1.29	99.47	9.84	1.40										
I1036/11	48.46	1.41	15.29	4.51	6.11	0.17	8.6	10.7	2.81	0.33	0.15	1.08	99.62	10.17	1.18										
I1036/15	48.86	1.35	15	5.35	4.96	0.16	8.08	10.64	2.88	0.5	0.16	1.53	99.47	9.78	1.21	11	92	27	8.7	160	40	270	140	260	1.32
I1036/16	48.9	1.34	15.61	5.2	5.03	0.15	7.9	10.67	2.97	0.19	0.14	1.2	99.3	9.71	1.23										
I1036/17	48.86	1.29	15.39	3.88	5.21	0.16	8.8	10.63	2.85	0.39	0.15	1.72	99.33	8.70	0.99										
I1036/38	48.9	1.38	16.26	3.8	5.03	0.15	8.24	10.94	2.86	0.44	0.15	1.38	99.53	8.45	1.03	7.7	100	26	5.6	180	9	240	150	310	0.85
I1036/4	48.82	1.46	15.48	3.83	6.18	0.17	8.66	10.68	2.61	0.32	0.17	1	99.38	9.63	1.11										
I1036/9	48.9	1.43	15.35	3.95	5.96	0.17	8.54	10.53	2.93	0.37	0.17	1.26	99.56	9.52	1.11										
I1037/1	49.96	1.57	15.88	3.04	6.11	0.17	7.21	10.54	3.09	0.4	0.17	1.34	99.48	8.85	1.23	7.7	110	33	5.5	140	56	290	78	180	0.77
I1037/3	50.04	1.61	13.21	7.67	5.03	0.17	7.01	10.36	3.1	0.44	0.17	0.9	99.71	11.93	1.70										
I1037/4	49.84	1.59	15.05	3.59	6.83	0.18	7.39	10.08	3.06	0.37	0.17	1.16	99.31	10.06	1.36										
I1037/5	50.4	1.46	15.31	4.31	5.28	0.16	6.87	10.75	3.07	0.44	0.16	1.25	99.46	9.16	1.33										
I1046/1	49.03	1.57	15.99	2.99	6.77	0.16	7.88	10.96	2.76	0.4	0.2	0.83	99.54	9.46	1.20	13	110	29	5.9	180	9	310	110	290	1.30
I1057/2	46.75	2.32	15.32	4.86	6.06	0.11	7.63	11.08	3.03	0.58	0.31	1.45	99.5	10.43	1.37	29	140	32	8.2	320	200	410	120	260	2.28
I1057/3	46.14	2.31	15.61	4.54	6.03	0.16	8.3	11.42	2.89	0.58	0.31	1.62	99.91	10.12	1.22	29	140	29	5.2	350	260	320	130	310	2.28
I1057/4	46.76	2.33	15.89	4.62	5.37	0.1	6.9	10.94	3.13	0.73	0.3	2.41	99.48	9.53	1.38	28	150	31	11	320	250	350	92	220	2.05
I1057/11	45.32	2.46	15.84	4.89	5.96	0.22	7.8	11.62	2.81	0.42	0.33	2.16	99.83	10.36	1.33	28	150	34	5.4	320	230	430	100	250	2.05

Analyses performed at the Chemical and Analytical Laboratory, Geological Institute of the Russian Academy of Sciences, Moscow. Major components were measured by wet chemistry (T. N. Tsepkova, N. L. Kalashnikova, E. V. Cherkasova, M. I. Stepanets, V. V. Karpushina, I. V. Kislova, G. A. Granovskaya, and M. V. Rudchenko, analysts) and trace elements, by XRF with in-house concentrations procedures (E. P. Shevchenko, analyst).

Table 3. Composition of representative chilled basaltic glasses (wt%) from the Sierra Leone region

Sample	SiO_2	TiO_2	Cr_2O_3	Al_2O_3	FeO	MnO	MgO	CaO	Na_2O	K_2O	P_2O_5	Total	K_2O/TiO_2
S2230/1-1	51.28	1.78	0	14.74	10.59	0.172	6.88	10.15	2.99	0.137		98.72	0.42
S2238/26-1	51.89	1.49	0.033	15.41	9.76	0.158	7.58	10.88	2.96	0.09		100.23	0.33
S2238/29-2	52.16	1.47	0	14.82	9.76	0.197	7.53	10.94	2.81	0.059		99.75	0.22
S2238/30-1	50.79	1.54	0.019	14.91	9.2	0.162	7.95	10.56	2.89	0.08		98.1	0.29
S2238/39-1	51.77	1.41	0.006	14.77	9.35	0.175	7.79	10.8	2.72	0.067		98.86	0.26
S2239/1-1	51.91	1.38	0.017	15.04	8.84	0.158	8.09	11.54	2.57	0.046		99.59	0.18
S2239/2-1	50.55	1.34	0.048	15.17	8.84	0.188	7.84	11.33	2.63	0.056		97.98	0.23
S2244/50-3	50.22	1.62	0.046	14.91	9.42	0.147	8.29	10.62	2.84	0.101		98.21	0.34
S2244/51-2	51.06	1.48	0.038	15.04	8.89	0.173	8.29	10.96	2.73	0.102		98.76	0.38
S2244/84-1	50.75	1.66	0	14.9	9.37	0.159	8.14	10.5	2.82	0.099		98.41	0.33
S2246/1-2	50.57	1.68	0.037	15.38	9.62	0.18	7.52	10.48	3.2	0.085		98.75	0.28
S2246/2-2	50.38	1.71	0.019	15.37	9.46	0.166	7.6	10.4	3.22	0.11		98.44	0.35
S2246/3-3	50.85	1.68	0.009	15.29	9.48	0.152	7.35	10.6	3.26	0.105		98.77	0.34
S2246/5-2	50.81	1.72	0.001	15.42	9.53	0.177	7.56	10.5	3.16	0.094		98.97	0.3
I1003/02-1	49.96	1.52	0.058	15.47	9.53	0.205	8.39	10.69	2.96	0.058	0.076	98.917	0.21
I1003/03-2	49.9	1.37	0.056	16.55	8.87	0.136	8.03	10.54	3.11	0.257	0.098	98.917	1.03
I1003/14-2	49.69	1.4	0.046	16.44	8.54	0.162	8.31	10.53	3.17	0.272	0.131	98.691	1.07
I1011/01-1	50.43	1.83	0.054	15.74	9.65	0.154	5.48	12.53	2.94	0.118	0.14	99.066	0.35
I1012/01-3	50.86	1.54	0.064	15.57	9.18	0.149	7.8	10.71	2.62	0.118	0.062	98.673	0.42
I1016/01-1	50.36	1.48	0.032	15.48	8.91	0.175	8.42	10.84	2.78	0.136	0.075	98.688	0.51
I1016/05-1	50.55	1.54	0.034	15.25	8.7	0.181	8.55	10.62	2.53	0.132	0.096	98.183	0.47
I1019/05	51.17	1.39	0.076	15.11	8.6	0.147	8.01	11.58	2.54	0.111	0.056	98.79	0.44
I1019/12	51.06	1.27	0.028	15.74	8.09	0.166	8.49	11.51	2.58	0.104	0.038	99.076	0.45
I1019/20-1	50.82	1.41	0.061	15.41	8.45	0.161	8.14	11.47	2.3	0.099	0.044	98.365	0.39
I1026/01-1	51.34	1.6	0.038	14.93	8.96	0.143	7.37	11.04	2.77	0.182	0.076	98.449	0.63
I1026/03-1	51.06	2	0.055	14.3	11.26	0.214	6.41	9.98	2.64	0.159	0.163	98.241	0.56
I1026/04-1	51.42	1.59	0.032	14.85	9.33	0.164	7.38	10.94	2.8	0.162	0.083	98.751	0.6
I1026/07-1	51.08	1.97	0.031	13.99	11.35	0.187	6.47	10.03	2.69	0.163	0.138	98.099	0.46
I1026/56F	51.53	1.74	0.03	14.3	11.06	0.173	6.87	10.36	2.57	0.175	0.11	98.918	0.55
I1026/57A-1	51.39	1.59	0.02	15.16	9.69	0.128	7.55	11.16	2.82	0.168	0.108	99.784	0.58
I1027/01-1	51.3	1.63	0.022	14.57	10.77	0.17	7.33	10.54	2.74	0.109	0.098	99.279	0.37
I1027/02-1	51.6	1.41	0.05	15.01	9.62	0.163	7.67	11.27	2.7	0.091	0.066	99.65	0.35
I1027/06	51.41	1.61	0.017	14.67	11.1	0.182	7.59	10.51	2.6	0.135	0.089	99.913	0.46
I1027/09-2	50.94	1.64	0.028	14.44	10.71	0.147	7.49	10.54	2.86	0.139	0.084	99.018	0.47
I1012/01-3	50.86	1.54	0.064	15.57	9.18	0.149	7.8	10.71	2.62	0.118	0.062	98.673	
I1030/01A-1	50.29	1.48	0.046	15.4	8.72	0.147	8.32	11.47	2.91	0.129	0.033	98.945	0.48
I1031/01-1	51.85	1.56	0.029	14.86	10.26	0.168	7.21	10.89	2.54	0.13	0.063	99.56	0.46
I1032/53-1	50.83	1.61	0.034	14.68	10.73	0.161	7.48	10.63	2.44	0.123	0.054	98.772	0.42
I1036/04-2	50.52	1.46	0.017	15.49	9.65	0.165	8.08	11.27	2.74	0.226	0.082	99.7	0.82
I1036/07-1	50.79	1.33	0.076	15.36	9.38	0.174	8.1	11.88	2.64	0.243	0.091	100.064	1
I1037/02-1	51.23	1.56	0.027	15.03	10.11	0.172	7.26	11	2.71	0.209	0.119	99.427	0.74
I1039/01-1	51.04	1.39	0.055	15.07	9.87	0.164	7.9	11.36	2.71	0.137	0.039	99.735	0.54
I1039/07	50.53	1.5	0.037	14.96	9.72	0.162	7.71	11.5	2.6	0.132	0.049	98.9	0.46
I1039/11	50.75	1.42	0.045	15.07	9.81	0.159	7.71	11.39	2.78	0.136	0.057	99.327	0.53
I1039/17	50.51	1.43	0.022	15.09	9.72	0.16	8.2	11.47	2.53	0.105	0.055	99.292	0.4
I1045/01-1	50.2	1.38	0.051	15.37	9.52	0.162	8.22	11.45	2.69	0.092	0.037	99.172	0.37
I1045/12-2	50.01	1.18	0.067	15.29	8.83	0.193	8.44	11.63	2.34	0.072	0.053	98.105	0.34
I1045/13-1	50.29	1.2	0.072	16.12	8.95	0.16	8.64	11.59	2.65	0.098	0.053	99.823	0.45
I1055/1-1	50.73	1.74	0.015	15.05	9.98	0.143	7.03	11.2	2.94	0.155	0.319	99.29	0.49
I1055/7	50.51	1.74	0.015	14.6	9.83	0.178	7.35	11.21	2.65	0.186	0.313	98.58	0.59
I1068/10-1	51.23	1.64	0.039	15.28	9.2	0.167	7.15	11.12	3.04	0.191	0.231	99.29	0.64
I1068/11-2	50.25	1.51	0.04	15.3	9.21	0.161	7.38	10.7	2.94	0.192	0.299	97.98	0.7
I1068/9-2	50.52	1.6	0.002	15.01	9.67	0.181	7.29	10.62	3.14	0.118	0.295	98.46	0.41
I1069/1-1	50.41	1.71	0	14.4	10.31	0.205	7.58	10.21	3.12	0.173	0.35	98.46	0.56

Table 3. Continued

Sample	SiO_2	TiO_2	Cr_2O_3	Al_2O_3	FeO	MnO	MgO	CaO	Na_2O	K_2O	P_2O_5	Total	K_2O/TiO_2
I1069/3-1	50.58	1.71	0.007	14.32	10.54	0.184	7.63	10.2	3.09	0.172	0.309	98.74	0.55
I1069/63-1	50.86	1.74	0.003	14.72	10.54	0.209	7.38	10.26	3.14	0.134	0.338	99.32	0.42
I1072/1-1	50.7	1.19	0.042	15.58	8.91	0.17	8.12	11.85	2.64	0.085	0.227	99.51	0.39
I1072/7-1	50.51	1.33	0.028	15.54	9.01	0.143	7.91	11.56	2.76	0.103	0.272	99.17	0.43
I1003/01-2	50	1.38	0.05	16.39		0.141	7.89	10.88	2.87	0.261	0.123	98.845	

Measurements were carried out on a Camebax-micro ion microprobe at the Analytical Center of the Joint Institute of Geology, Geophysics, and Mining, Siberian Branch of the Russian Academy of Sciences, Novosibirsk.

and its $(La/Sm)_n$ ratio also being considerably higher (0.80). Therefore, this sample is similar to T-MORB tholeiites [*Sun et al.,* 1979].

Stations 1016, 1039, 1038, 1029 and 1030, in a sequence from west to east, make a sampling profile transverse to the strike of the rift. With a certain degree of approximation, it can be ascertained that all the basalts representing the crestal zone in the Northern domain are closely similar. A characteristic feature of this population is the sharp predominance of high-Mg basalts, which are seldom encountered in the MAR axial zone. At the same time, compositions of basalts characterizing various morphostructures of this zone display three types of distinctions. Firstly, one observes variations in the abundances of titanium and sodium suggesting that these basalts originated from compositionally distinct initial melts. Against the overall trend of increasing titanium contents, one may discriminate basalt types from Station 1072, Station 1019, and Station 1016. In the TiO_2 vs. FeO/MgO plot (Figure 3b), basalts of these stations cluster in separate groups, each providing an origin to an independent low angle differentiation trend. Overall, potassium, phosphorus, and sodium contents increase along this trend as well. Distinctions of a second type are expressed in that the basalts show variable degrees of potassium enrichment independent of their titanium contents or differentiation degrees, as can be seen in the K_2O vs. FeO/MgO plot (Figure 3f). The more potassic varieties are encountered at the flanks, with the highest potassium contents being recorded in basalts from the eastern flank. Flank basalts are also characterized by higher contents of incompatible elements. Distinctions of a third type are expressed in the variable differentiation degrees of the basalts. Evolved basalts are considerably more widespread at the eastern flank. This might indicate that prior to the aforementioned change in the geo-

Table 4. Rare-earth element contents (ppm) in selected basalts from the Sierra Leone region

Sample	La	Ce	Nd	Sm	Eu	Tb	Yb	Lu
S2246/2	5	13	12	4.7	1.3	0.94	3.8	0.61
S2234/24	3.8	10	8.1	2.7	0.94	0.61	2	0.31
S2230/1	5.2	16	13	4.3	1.4	1.2	3.8	0.57
S2238/3	5.4	14	13	4.7	1.3	1.1	3.8	0.59
S2239/1	3.2	8.6	7.9	3.1	0.9	0.68	2.6	0.41
S2244/50	4.3	12	11	3.8	1.4	1.1	3.4	0.54
I1003/2	3.3	11	10	3.9	1.4	1.1	3.4	0.54
I1003/4	5.9	16	11	3.2	1.1	0.73	2.7	0.45
I1026/23	3.4	10	9.1	3.6	1.2	1.1	3.4	0.53
I1027/5	5.2	16	13	4.5	1.5	1.2	4.0	0.64
I1029/1	3.8	11	8.4	2.8	1.1	0.73	2.4	0.38
I1031/1	4.2	12	10	3.5	1.2	0.92	2.9	0.46
I1036/15	8.9	21	13	3.7	1.3	1.3	2.6	0.38
I1037/3	6.7	18	13	4.1	1.4	1.4	3.1	0.49
I1039/1	4.0	11	9.5	3.4	0.98	0.98	3.0	0.43
I1045/1	3.9	12	9.5	3.1	1.1	1.1	2.3	0.28
I1046/1	11	25	15	4.0	1.2	1.2	2.9	0.42
I1057/2	22	48	26	5.6	1.6	1.2	2.9	0.42
I1057/3	23	52	25	5.1	1.6	1.2	2.3	0.33
I1057/4	22	53	26	5.5	1.6	1.2	2.9	0.41
I1057/11	25	52	27	6.5	1.9	1.2	3.4	0.52

Measurements using INAA were carried out at the Chemical and Analytical Laboratory, Geological Institute of the Russian Academy of Sciences, Moscow (S. M. Lyapunov and A. V. Gorbunov, analysts).

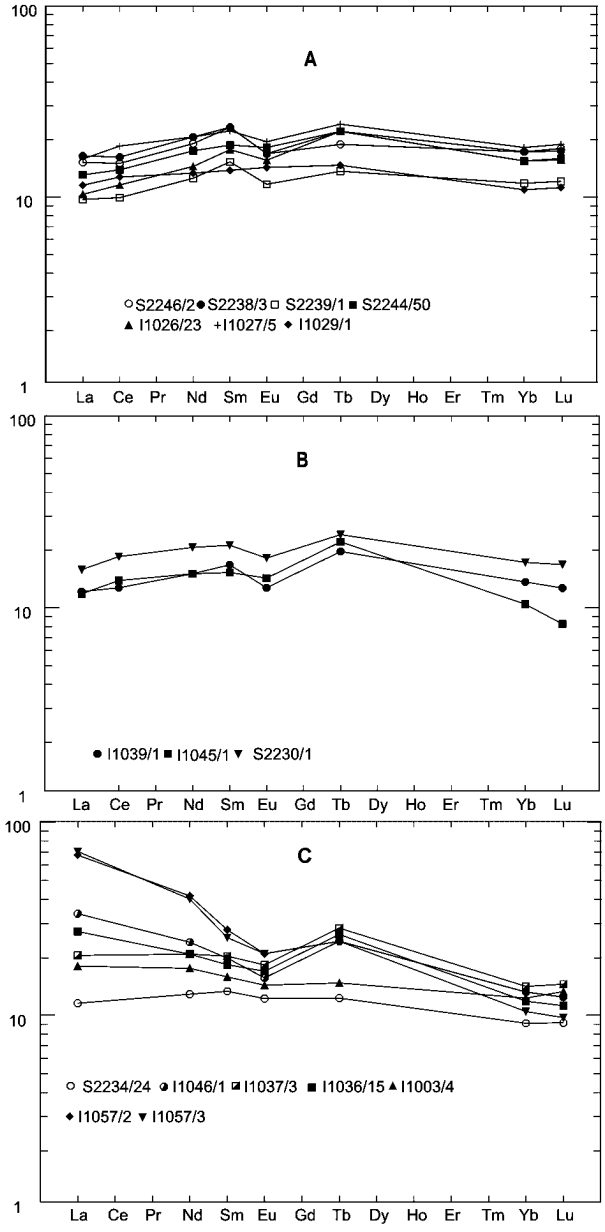

Figure 2. REE spectra for basalts from (a) stations north of the Sierra Leone FZ, (b) stations south of the Sierra Leone FZ, and (c) enriched tholeiitic and alkaline basalts. Chondrite values from [*Evensen et al.,* 1978].

dynamic regime of spreading, there existed more favorable conditions for basaltic melt differentiation.

Within the Near-FZ domain, basalts characterize the following rift-related structures: a neovolcanic rise (Station 2246), a minor rise in the sinistral strike slip zone that bounds the Near-FZ domain (Station 2244), and the western slope of the rift valley (Station 2247). Their feature in common with the Northern domain basalts is their high MgO content (8.04–8.78%). However, they differ from the rift basalts of the Near-FZ domain in that the latter are perceptibly higher in Ti and Fe, compared even to Station 1016 basalts, at virtually the same concentrations of potassium and phosphorus. This is readily apparent from the TiO_2 vs. FeO/MgO plot (Figure 3b), where these basalts make an independent, the highest-Ti group among the high-Mg basalts. Within this group, the basalts are also differentiated in that those characterizing the structures closest to the Bogdanov FZ (Stations 2244, 2247) are considerably higher in sodium. Therefore, in the Near-FZ domain, widespread are two types of modern basalts derivative from distinct initial melts: Station 2244–type (relatively high-Ti (1.50–1.78% TiO_2) and high-Fe (9.11–10.31% FeO^*) basalts) and Station 2246–type (high-Ti (1.76–1.78% TiO_2), high-Fe (9.57–10.85% FeO^*), and high-Na (3.03–3.09% Na_2O) basalts).

The above compositional features of rift-related basalts from the Near-FZ domain are replicated in their chilled glass compositions, although one should note the existing compositional difference between the basalts and their glasses. As in all the instances mentioned, glasses are less magnesian and less high-Ti (1.45–1.72% TiO_2) than their basalts, while glasses from Station 1046 are also higher in sodium (3.09–3.26% Na_2O).

In terms of trace element concentrations, these rift-related basalts are distinguished from the rift-related basalts of the Northern domain and are close to the flank basalts of the Northern domain: 3.1–5.3 ppm Nb, 1.4–2.4 ppm Rb, $(Nb/Zr)_n$ = 0.34–0.54. Their REE spectra are typical of depleted tholeiitic basalts with $(La/Sm)_n$ = 0.55–0.62 and slight negative Eu anomaly (Figure 2a).

Both types of basalts thus discriminated have not been encountered at the flanks of the Near-FZ domain. At the western flank, recorded were basalts resembling Station 1016 type (Station 1012 type). Glasses from these stations are also similar in composition. At the eastern flank, by contrast, encountered are comparatively low-Ti and high-Mg basalts (8.24–9.18% MgO), also having elevated contents of calcium (Stations 1009, 1010). Their titanium contents are generally lower than in Station 1072 basalts. Therefore, Station 1010 basalts can be classified as an independent, lowest-Ti type (0.97–1.01% TiO_2). This basalt type is also featured by very low incompatible element contents (1.5–1.7 ppm Nb, 55–63 ppm Zr, 21–23 ppm Y, 1.3 ppm Rb), a low $(Nb/Zr)_n$ ratio (0.26–0.34), and very high Cr contents (420 ppm) and Ni abundances (220 ppm).

North of the Bogdanov FZ, basalts are encountered in the nodal basin and on the slopes of the Northern transverse ridge. Basalts from the nodal basin (Station 1003) are distinguished from all the basalts discussed earlier in that their dominant varieties have lower MgO contents (7.11–7.71%) and higher differentiation coefficients FeO^*/MgO (1.09–1.30). Another characteristic feature is their appreciably higher contents of sodium oxide (3.18–3.54% Na_2O) and potassium oxide (0.30–0.39% K_2O), due to which on the variation diagrams Na_2O vs. FeO/MgO and K_2O vs. FeO/MgO (Figures 3e, 3f) these basalts plot in independent fields differing perceptibly from the other basalts. Compositions of basaltic glasses from this station are generally close to basaltic compositions in terms of their Ti and Mg contents, but are distinguished by their lower contents of Na_2O (2.72–3.17%) and somewhat lower K_2O abundances

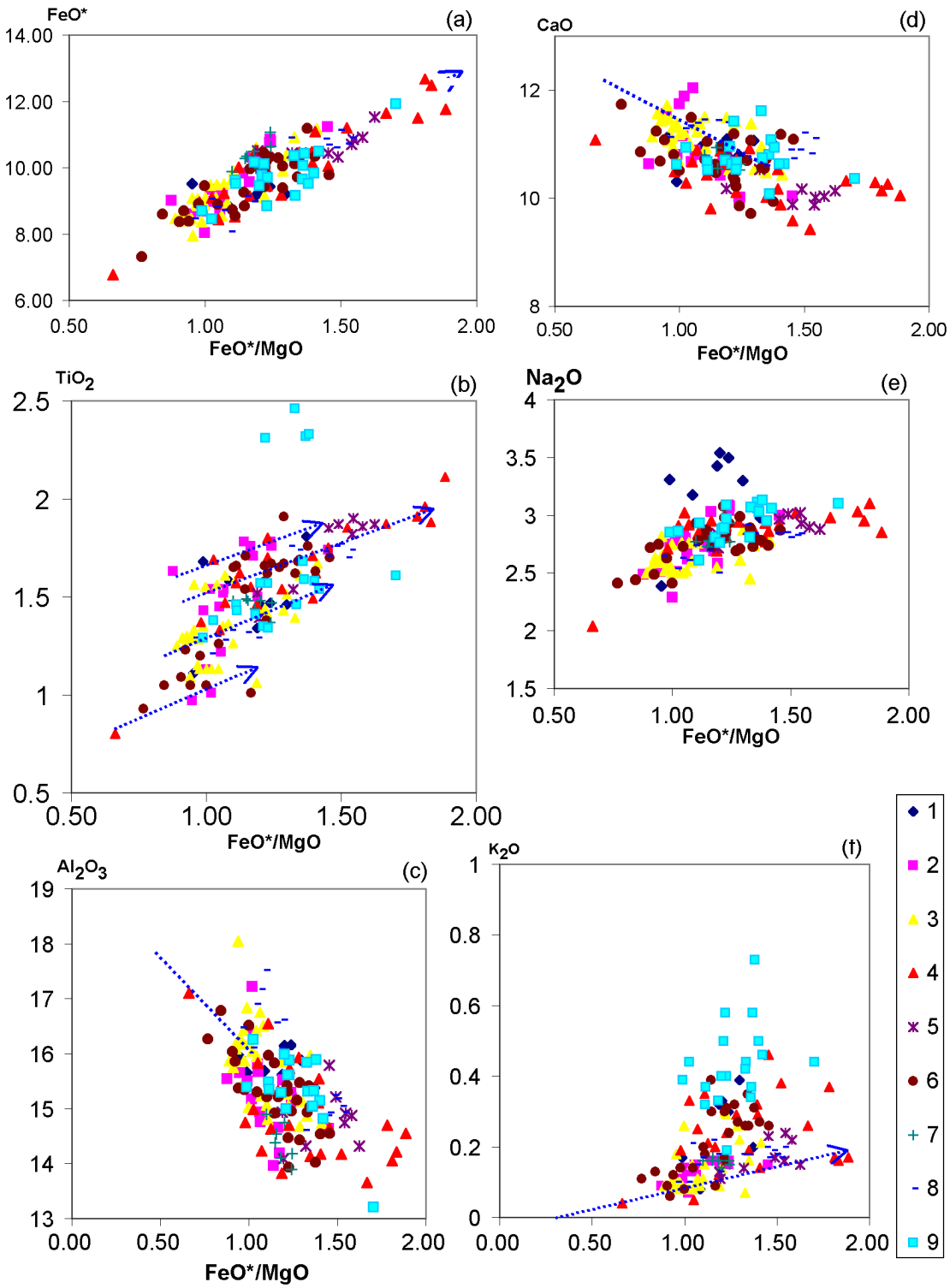

Figure 3. Variation diagrams for major oxides in basalts vs. the fractionation coefficient FeO*/MgO. Dashed arrows depict differentiation trends. Symbols (basalts from): 1 – Bogdanov FZ, 2 – Near-FZ domain, 3 – Northern domain, 4 – "Ore" survey area, 5 – 1st Southern domain, 6 – Markov Basin, 7 – 2nd Southern domain, 8 – 3rd Southern domain, 9 – Southwest domain.

(0.16–0.31%). These basalts also have markedly higher contents of incompatible elements, such as Nb (7.9 ppm), Rb (4.8 ppm), and Sr (260 ppm), although their Zr and Y contents (100 ppm and 25 ppm, respectively) are comparatively low. Their Cr and Ni contents (290 ppm and 150 ppm, respectively) are also relatively low. The relatively high ratios $(Nb/Zr)_n = 0.87$ and $(La/Sm)_n = 1.08$ in the basalts and the K/Ti ratio (up to 1.24) in glasses permit classing these basalts with T-MORB-like enriched tholeiites.

The collection of basalts from this structure contains a single sample (1003/2), which, despite its high sodium contents, is low in potassium and higher in magnesium, and it has a low $(La/Sm)_n$ ratio (0.48).

Compositions of basalts from the Northern transverse ridge are broadly variable. Station 1005 basalts are very high in Mg. Sample 1005/1 has many parameters (except its higher Na_2O) in common with Station 1046–type basalts from the neovolcanic rise. Sample 1005/39 differs sharply from the latter, its parameters being closest to Station 1072–type basalts. Compositions of Station 1011 basalt and its glass are also closest to the neovolcanic rise basalts. Unlike the latter, it is lower in MgO. Note that Station 1011 is confined to the slope of the depression that bounds the Northern transverse ridge on the east. This depression occurs on trend with the neovolcanic rise, forming its immediate northwesterly extension, which, judging by the compositional similarity of the volcanic products making these morphostructures, might be indicative of their structural or genetic links.

The broadest compositional diversity features basalts from the "Ore area." Unlike all the above groups, this basaltic population shows a wide range of MgO (6.24–8.91%) accompanied by a broad range of fractionation coefficients ($FeO^*/MgO = 0.80–1.89$). Basalts with high MgO contents are sparse in number. In terms of titanium contents, basalts from the "Ore area" come in two groups, either forming a differentiation trend of its own. In the higher-Ti suite (Samples 1022/5, 6, 1025/1, 2, 4, 8, 1026/20, 21, 24, 25, 1027/1, 3, 4, 5, 7, 1028/18), the highest-Mg basalts (Samples 1027/4, 7, 1028/18) have many parameters that are similar to Station 1016–type basalts, forming jointly with the latter a continuous differentiation trend on the TiO_2 vs. Fe/MgO plot (Figure 3b). In the most evolved varieties of this group, titanium contents are as high as 1.91–2.10% (Samples 1022/5, 1025/1). In the lower-Ti basalt suite (Samples 2234/23, 1022/2, 1026/1, 2, 8, 10, 1027/2), the lowest-Ti Sample 1022/2 has many parameters, except for its considerably higher sodium content, rendering it closely similar to Station 1072–type basalts. The other most primitive basalts from this suite (Samples 2234/23, 1027/2) are close to Station 1019–type basalts, also differing from the latter in having higher sodium contents, forming jointly with them a continuous differentiation trend on the TiO_2 vs. Fe/MgO plot (Figure 3b). Another characteristic feature of the basaltic population from the "Ore area" is that some of them are enriched in potassium. This property is shared by the basalts of the high-Ti and low-Ti suites alike. As is seen from the K_2O vs. FeO/MgO plot (Figure 3f), the majority of basalts from the Sierra Leone region plot in a field with a trend of slight potassium enrichment with advancing differentiation. The most evolved sample has 0.26% K_2O. Above this field, there plot several basaltic groups with higher potassium contents at a given fractionation degree. Some basalts from the "Ore area" plot within these fields as well. Potassium abundances in enriched basalts from the "Ore area" range from 0.20% (Sample 1026/1) to 0.46% (Sample 1027/5) irrespective of any other parameters. Note, however, that the enriched varieties are dominantly the more evolved basalts.

Compositional variations in glasses recovered from the "Ore area" are governed by the same regularities as basaltic compositional variations. Overall, however, the measured glass compositions differ from their host basalts in having lower magnesium, sodium, and potassium contents. Among the glasses, detected has been a sample (1026/6) with very high magnesium (10.08% MgO) and very low titanium (0.67% TiO_2), sodium (2.25% Na_2O), and potassium (0.02% K_2O) contents, rendering it close to Station 1010–type basalts.

In terms of trace element contents, the higher-Ti and lower-Ti varieties are not distinguished from each other and are overall close in this respect to Station 1016 basalts, except for their considerably lower contents of Ni (78–130 ppm) and Cr (180–290 ppm). It is worth noting the mismatch of certain major- and trace element parameters in a number of samples from the "Ore area." Thus, the most potassic Sample 1026/1, although its composition is somewhat enriched (judging from $(La/Sm)_n = 0.68$, compared to Sample 1026/23 with $(La/Sm)_n = 0.55$)), it still remains within the N-MORB type, whereas based on its potassium content it can be classed with T-MORB. Likewise, Sample 1025/1 has a potassium content placing it with T-MORB, albeit its $(Nb/Zr)_n$ ratio is low (0.41).

Basalts representing various structural features south of the Sierra Leone FZ have distinct compositional variations patterns that differ from segment to segment. Within the 1st Southern domain, adjoining the Sierra Leone FZ, basalts from Stations 2230 and 1031 jointly form a relatively highly evolved suite, similar in many of its parameters to its correlative high-Ti suite from the "Ore area." This regularity is also pronounced at the level of chilled glass compositions. Some basalts from Station 2230 (Samples 2230/1, 3, 6) are very slightly enriched in potassium (0.22–0.24% K_2O). Their incompatible trace element contents are slightly higher than in Station 1016 basalts, although generally they are closely similar. Judging from their ratios $(La/Sm)_n = 0.63–0.77$ and $(Nb/Zr)_n = 0.49–0.52$, these basalts are derivatives of depleted tholeiitic melts enriched insignificantly in lithophile elements. The REE spectra for these basalts show marked negative Eu anomaly (Figure 2b).

Among the basalts composing the deep rift basins (Markov and the 5°46′), one finds sporadic samples resembling high-Mg low-potassic varieties of the low-Ti suite from the "Ore area" (Sample 1032/22). The rest of the basalts constitute a relatively highly evolved suite with MgO contents in the range 6.72–8.60%. In its basic parameters, this suite resembles the high-Ti suite in the "Ore area." Unlike the latter, the dependency of titanium contents on magnesium is not marked as strongly. The basalt population from the Markov Basin also shows random variations in sodium contents. Thus, the high-Mg Sample 1032/29 has a relatively high sodium content (3.08% Na_2O) and, by contrast, the

low-magnesian Samples 1032/40 and 1068/4, 5 are relatively low in sodium (2.71–2.74% Na_2O). As compared to the other rift basalts from the 1st Southern domain, the basalts from rift-related basins are more strongly enriched in potassium (0.24–0.39% K_2O). Variations in potassium, sodium, and titanium contents show no correlations. Similar parameters (except for potassium contents, whose measured values are perceptibly lower than in the basalts (0.14–0.21% K_2O)) are displayed by the chilled glasses recovered from the rift-related basins.

The Markov Basin basalts are comparatively low in nickel and chromium. Their contents of incompatible elements such as niobium and rubidium are elevated as compared to all the basalts mentioned above, except for those from the nodal basin of the Bogdanov FZ. The contents of these elements are highest in the most potassic basalts: 6.9 ppm Nb, 5.1 ppm Rb. Their $(Nb/Zr)_n$ and K/Ti ratios are also relatively high, up to 0.78 and up to 0.70, respectively. Therefore, these basalts are closely similar to T-MORB tholeiites.

The slopes of the basins and of their surrounding structural features yielded abundant dolerites, especially numerous at Stations 1060 and 1063. All the dolerites are characterized by very high magnesium contents (8.50–10.20% MgO) and overall low potassium and titanium abundances. The dolerites are subdivided into two groups. One group comprises dolerites with higher abundances of titanium, closely similar to Station 1019–type basalts. The dolerites of the other group are very low in titanium (0.93–1.09% TiO_2) and approximate Station 1010–type basalts.

Compositionally, the dolerites differ considerably from the young basalts from the rift-related basins described above. The dolerites predate these basalts, since they have been exhumed at the sea floor through tectonic processes. Consequently, the recent prehistory of these basins had an evolutionary phase geodynamically similar to those for the rift of the Northern domain.

Within the 2nd Southern domain, basalts characterizing the neovolcanic rise (Station 1039) are compositionally uniform and belong to high-Mg rocks. Overall, they are similar to the primitive varieties of the high-Ti suite from the "Ore area" (1.37–1.49% TiO_2, 4.9 ppm Nb, 2.2 ppm Rb), differing from the latter in having higher sodium (2.73–2.93% Na_2O) and potassium contents (0.14–0.17% K_2O). Glass compositions, according to most parameters except the perceptibly lower magnesium concentrations, resemble basaltic ones.

Within the 3rd Southern domain, sampling exercises covered two neovolcanic ridges set rather wide apart. The one farther north is represented by Station 1055 basalts, which have a wide range of magnesium contents, the other components ranging insignificantly and irrespective of magnesium ones. Overall, however, these basalts resemble the high-Ti basalts from the "Ore area." Except for the higher sodium contents, their glass compositions correspond to basaltic ones.

The basalts of another neovolcanic rise (Station 1045) are dominated by high-Mg varieties. In terms of their titanium, sodium, and trace element contents, these basalts and their glasses are closely similar to Station 1019–type basalts, differing from the latter in their somewhat elevated potassium and rubidium contents.

The Southwest outcrop area of basalts has been sampled extensively enough. A feature common to basaltic compositions under study is their high content of potassium. Predominant are varieties with $K_2O > 0.35\%$ (up to 0.50%). Basalts from most stations in the Southwest outcrop area (Stations 1036, 1037, 1046) are closely similar, jointly comprising a suite with a wide range of MgO (6.87–8.54%), the other elements correlating with it (Figure 3). Except for sporadic samples, this suite resembles the low-Ti suite from the "Ore area," although unlike the latter it is higher in sodium (2.81–3.09% Na_2O), phosphorus, zirconium (92–120 ppm), niobium (7.7–14 ppm), and rubidium (6.6–8.7 ppm) (Figures 3e, 4a, 4b, 4c, 4d). The behavior of potassium does not depend on magnesium variations. High potassium contents are characteristic of both high-Mg varieties and relatively low magnesian ones alike. The glasses are compositionally similar to their respective basalts, except for their perceptibly lower potassium contents. But potassium contents of glasses from the Southwest outcrop area are higher than those of glasses from the other domains of the Sierra Leone region (0.21–0.24% K_2O), the K/Ti ratio being high (0.63–1.0) as well.

Based on their $(Nb/Zr)_n$ ratios, generally very high, these basalts are discriminated into T-MORB-like and P-MORB-like tholeiites. The former comprise Samples 1036/38 and 1037/1 with $(Nb/Zr)_n = 0.77–0.85$, and the latter, Samples 1036/1, 1036/15, 1046/1 with $(Nb/Zr)_n = 1.28–1.32$. Such a discrimination is further supported by the character of the REE spectra (Figure 2c). Samples 1036/16 and 1037/3 with $(La/Sm)_n = 0.93–0.96$ represent T-MORBs, and Sample 1036/15 with $(La/Sm)_n = 1.42$, P-MORB.

In sharp contrast to all the aforementioned basalts, are the basalts from the northernmost station in the Southwest outcrop area, Station 1057. These are distinguished by the highest contents of potassium (0.42–0.73% K_2O), titanium (2.31–2.46% TiO_2), and phosphorus (0.30–0.33% P_2O_5) and reduced contents of silica (45.32–46.76% SiO_2) (Figures 3b, 3f, 4a, 4b, 4c, 4d). On the diagram ($Na_2O + K_2O$) vs. SiO_2 (Figure 4e), these basalts plot in the alkaline basalt field of [*Irvine and Baragar,* 1971]. Among trace elements, sharply elevated contents, as compared to the aforementioned basalts, are shown by niobium (28–29 ppm), strontium (320–350 ppm), barium (200–260 ppm) (Table 2) and the light REE (Table 4), the ratios $(Nb/Zr)_n = 2.05–2.28$ and $(La/Sm)_n = 2.28–2.69$ also being very high. The REE curves are sharply elevated in the light REE region, whereas in the medium REE and heavy REE regions these curves are close to those for the basalts described above (Figure 2c).

Discussion

One of the principal compositional features of the basalts spread in the vicinity of the Sierra Leone FZ is the wide, almost ubiquitous occurrence of relatively high magnesian basalts. The low contents of potassium and lithophile trace elements, low $(Nb/Zr)_n$ and $(La/Sm)_n$ ratios, and REE patterns for most of these basalts suggest that they are derivatives of depleted N-MORB-like tholeiitic melts. Despite

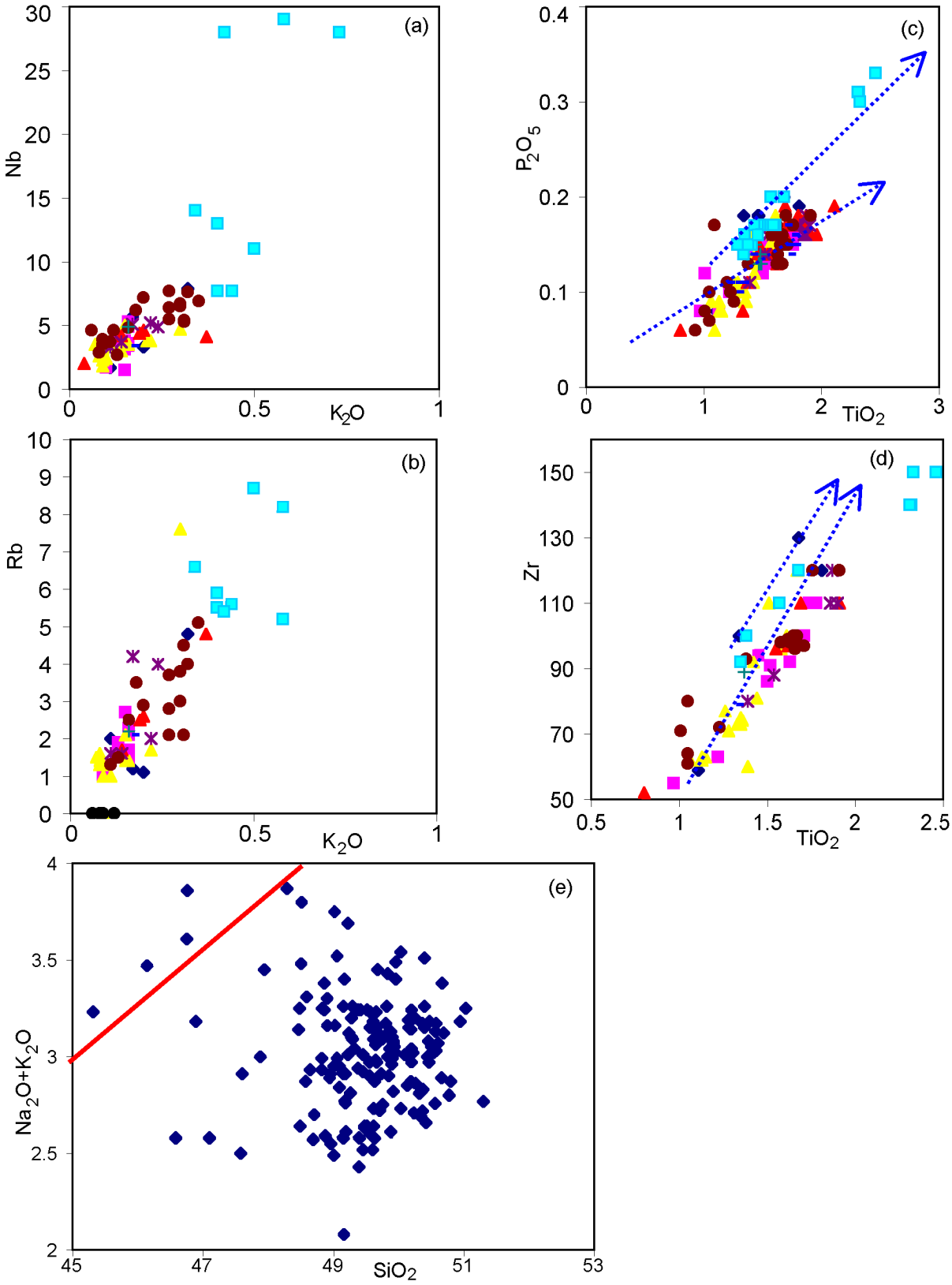

Figure 4. Variations diagrams for trace elements and oxides in basalts from the Sierra Leone region. Symbols, as in Figure 3. Figure 4e shows the boundary line as per [*Irvine and Baragar*, 1971] between alkaline (above) and tholeiitic (below) basalts.

their high-magnesian composition, all the basalts have undergone some degree of fractionation, as evidenced by their REE spectra (Figures 2a, 2b) showing marked negative Eu anomaly. Using an approach published earlier [*Schilling et al.,* 1995], we have estimated the parameters of mantle melting responsible for the initial melts to form. Data thus obtained provided the basis for model calculations for the magmatic system using COMAGMAT software package [*Ariskin and Barmina,* 2000; *Ariskin et al.,* 1993]. In terms of MgO content (a maximum of ca. 20.2 wt% has been recorded for Station 1019 basalts), the initial melts corresponded to picrobasalts, to evolve en route to the ocean floor surface, with their SiO_2 content increasing progressively and their magnesium content decreasing to the level of olivine basalts.

Within this group, basalts show variations in the contents of titanium, sodium, and potassium independent of their magnesium contents (Figures 3b, 3c, 3e, 3f). Overall, the variations in, and contents of, titanium, sodium, and potassium are not interdependent. Not infrequently, basalts discriminated according to the above major element parameters constitute tight groups and represent different morphostructures. This implies that these tight groups represent various basalt types with distinct conditions of origin. In terms of titanium concentrations, these types constitute the following suite, from lowest-Ti to highest-Ti ones: Station 1010 basalts, Station 1072 basalts, Station 1019 basalts and the low-Ti suite of the "Ore area," Station 1016 basalts and the high-Ti suite of the "Ore area," rift basalts of the Near-FZ domain, and Station 1057 alkaline basalts. On the TiO_2 vs. FeO/MgO plot (Figure 3b), basalts with dissimilar Ti contents make up independent fields with low-angle differentiation trends, but without sharp boundaries between each other, because there exist varieties with transitional compositions.

Basalts with closely similar titanium contents may differ perceptibly in terms of sodium contents, although generally basalts with elevated titanium contents are also higher in sodium. Based on sodium contents, basalt types established using titanium abundances may be further subdivided into independent types (or subtypes). Thus, among the basalt type close to Station 1019–type basalts, established is a succession from the lowest-sodium to highest-sodium basalts: Station 1019 basalts < the low-Ti suite of the "Ore area" < the Southwest domain (except for Station 1057) < Station 1003. Among the basalt type similar to Station 1016 basalts, established is a succession from the lowest-sodium to highest-sodium basalts: Station 1016 basalt and the high-Ti suite of the "Ore area" < Station 1039. Among the rift-related basalts of the Near-FZ domain, Station 1046 basalts are considerably higher in sodium than Station 1044 ones.

Within certain structural features, high-Mg basalts are associated with lower-magnesian varieties. Where basalts of the same type with variable magnesium contents are encountered (e.g., Station 2238 basalts), they show a systematic decrease in calcium and aluminum contents with increasing contents of iron, titanium, sodium, potassium, and phosphorus and with decreasing magnesium contents. Evidently, these systematic variations in basaltic compositions are due to crystal differentiation processes occurring in a magma chamber (in particular, olivine and plagioclase precipitation). Evolved basalts are relatively widespread in the nodal basin of the Bogdanov FZ, in the Southwest domain, in the Markov Basin, and they are also encountered at the eastern flank of the Northern domain. However, the most evolved basaltic suite is the one documented in the "Ore area." On variation diagrams (Figures 3a, 3c, 3d), the totality of evolved basalts form large fields, because they comprise many basalts of various types discussed above. Nonetheless, these large compositional fields show a vague tendency for a systematic decrease in calcium and aluminum contents and an increase in iron, titanium, sodium, potassium, and phosphorus contents with decreasing magnesium.

In those domains where basalts constitute relatively evolved suites, such as the nodal basin of the Bogdanov FZ, the "Ore area," the Markov Basin, and the Southwest domain, depleted basalts occur in association with basalts enriched in potassium and lithophile trace elements. In terms of their $(Nb/Zr)_n$ and $(La/Sm)_n$ ratios and REE patterns, these can be differentiated into derivatives of T- and P-MORB-like tholeiitic melts. The degree of the lithophile element enrichment of the basalts does not depend on their contents of magnesium, titanium, or sodium. The highest-potassic basalts are developed within the Southwest domain, where no depleted basalts have been recorded. This domain has also yielded alkaline basalts (Station 1057), differing from enriched tholeiitic basalts in that they have higher abundances of potassium, phosphorus, titanium, very high contents of niobium, strontium, and barium, as well as low silica contents. In view of these major- and trace-element parameters and a number of geological facts (namely, that the Southwest domain is the most uplifted one in the study region and the architecture of the crestal zone at this portion of the MAR is asymmetrical (showing the lack of basalts on its eastern flank)), it can be inferred that beneath the Southwest domain there takes place melting of a deep mantle material that rises in the form of a plume into the higher horizons of the upper mantle. Basalts that are closest to initial alkaline melts originating under plume impact have been recovered at Station 1057. The other basalts from the Southwest domain are likely to result from mixing of alkaline magmas and depleted melts generated beneath the rift zone. Since some basalts in the Markov Basin, spatially close to the Southwest domain, are also enriched in lithophile elements, it is evident that during their genesis their initial melts suffered influence from mantle plume material. Enriched basalts from the "Ore area" and the nodal basin of the Bogdanov FZ occur far enough from the Southwest domain, and they are separated by areas of volcanic activity devoid of enriched basalts. Apparently, near the "Ore area" and the Bogdanov FZ nodal basin, there may exist plume activity domains as yet to be discovered. In particular, one of these could be located east of the "Ore area," because some basalts at the eastern flank of the Northern domain are enriched in lithophile elements.

The impact from plume material localized beneath the Southwest domain is likely to manifest itself in compositions of rift-related basalts not only in the Markov Basin, but also in the other nearby rift-related domains, inasmuch as, generally, they are more evolved and have higher in potassium, sodium, and titanium at the same magnesium contents as

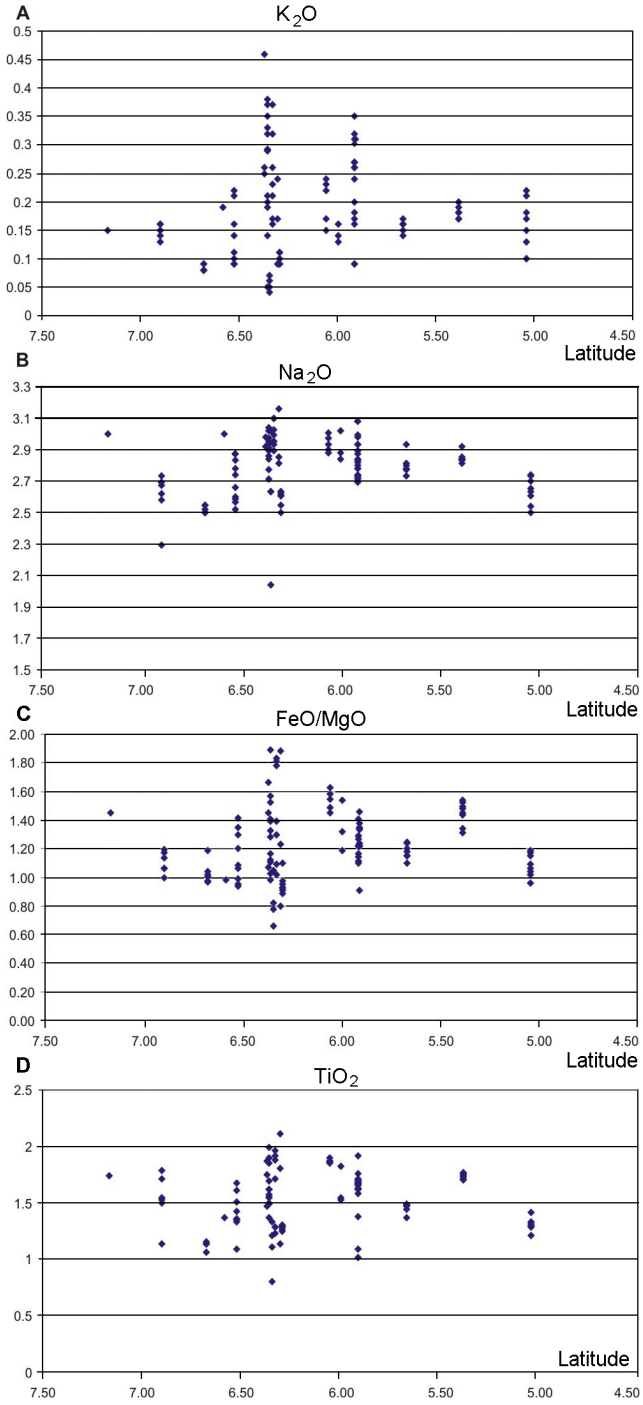

Figure 5. Variations and contents of K_2O, Na_2O, TiO_2 vs. FeO^*/MgO in basalts dredged from various portions of the rift valley.

their counterparts north of the Sierra Leone FZ (Figure 5).

In what way is this influence exerted? Is direct mixing of plume- and rift-related melts the case? Not only are the products of the parental plume melts high in lithophile elements, but they are also high in titanium. Meanwhile, enriched rift basalts can be either relatively high-Ti or low-Ti. Note also that in a number of cases rift-related basalts show no proportionate enrichment in different lithophile elements. This evidence is inconsistent with the melt mixing hypothesis. More convincing are those explanations of the facts observed that invoke the fluid transport mechanism. Assumedly, as the fluid-enriched plume material rises, the highly mobile volatiles travel into the overlying horizons ahead of the plume proper. The fluid can be enriched in lithophile elements with an elevated compatibility to fluid phase. In addition to radial effluence of fluid, it advances in the form of fluxes along high permeability zones in the tectonosphere. The inflow of fluid material results in a certain enrichment of rift-related basalts in lithophile elements, and fluid flows enrich the melts being generated beneath the Markov Basin.

What is the nature of the plume proper? *Schilling et al.* [1994] and others, based on their study of composition and isotope geochemistry of rift-related basalts in the vicinity of 1°–2°N, substantiated the existence of the long-lived Sierra Leone plume in this region. Its activity results in a chain of structural highs stretching from the MAR in a northeasterly direction toward Africa. A much smaller plume, whose evidence was described above, might be an offshoot of the Sierra Leone plume. There may be several such offshoots within the near-equatorial Atlantic.

As is readily apparent from the above, neither magma differentiation processes nor impact from active plume material can explain variations in the contents of titanium or sodium in basalts from the Sierra Leone region. The most likely cause of these variations is differences in the conditions of generation of their initial melts: temperature, depth of magma generation zone, and partial melting degree.

In order to establish the causes of variations in magma generation conditions, let us scrutinize the regularities of spatial distribution of the various basalt types. Each particular tectono-magmatic province here recognized, bounded mainly by sinistral strike slips or by the Bogdanov FZ, is characterized by a basalt type of its own. Consequently, beneath every such portion of the rift, there exists a subaxial diapir of asthenospheric mantle (asthenospheric high) with its peculiar, dissimilar from the neighboring ones, conditions of generation of basaltic melts. Each of the largest domains of the rift, as, e.g., the Northern domain or the 3rd Southern domain, accommodates at least two such asthenospheric highs. Magma generation conditions in these diapirs are non-steady-state and time changeable, as evidenced by compositional differences between the axial and flank basalts along the same profile across the crestal zone. There are structures (the "Ore area" and the Markov Basin (Figures 5b, 5d)) where magma generation conditions are particularly unstable, judging by the fact that these structures are composed of various types of basalts. As pointed out above, the formation of both these structures has been heavily influenced by the Sierra Leone FZ. Apparently, one of the causes for non-steady-state magma generation conditions are tectonic movements reaching from sea floor as deep as the magma generation zone.

The highest-Ti depleted basalts are widespread near the Bogdanov FZ. These same basalts are distinguished by their elevated sodium and iron contents. According to [*Klein and*

Langmuir, 1987], elevated sodium contents of basalts suggest a lower degree of partial melting for their initial melts, and an elevated iron content is due to a greater depth of the magma generation zone. According to [*Niu and Batiza,* 1994], these compositional features of Near-FZ domain basalts might be due to the effect from colder lithosphere of the opposite FZ wall on the melting process. This assertion is especially true of the basalts from the neovolcanic rise (Station 2246) jutting deeply into the Bogdanov FZ. Indeed, basalts characterizing this structure have elevated sodium contents. It is not unlikely that the elevated titanium contents of these basalts result from the influence from colder lithosphere of the opposite FZ wall. It is common knowledge that in near-FZ zones high-Ti gabbroic rocks are often widespread [*Pushcharovsky,* 1989; *Skolotnev,* 2003]. At the same time, at the flanks of the Near-FZ domain, basalts differ in composition from the rift-related basalts. Probably, the degree of influence from the FZ on the magma generation processes in the rift depends on the character of tectonic activity of the FZ proper, which may change through time. Nonetheless, it can me surmised that one of the reasons for variations in sodium and titanium contents might be tectonic movements bringing in contact lithosphere blocks with different temperatures at the level of magma generation.

Analyzing distribution of diverse basaltic types with distinct titanium and sodium contents reveals a marked prevalence of higher-Ti and higher-Na types south of the Sierra Leone FZ (Figures 5b, 5d). This is in keeping with the fact that nearby, in the same region there rises a deeper mantle plume. It was shown above that, as regards titanium contents, the plume material exerts no direct influence on rift-related melts. The same holds true of sodium, because sodium abundance in plume basalts is no higher than in rift-related basalts from southern domains. Nonetheless, the presence of a plume is the only significant factor that differentiates the conditions of generation of rift-related basalts from the northern and southern domains. This may imply that the plume, without exerting a direct influence on rift melts as regards sodium and titanium contents, does influence the temperature and depth conditions for magma generation, so that the resultant initial melts become enriched in titanium and sodium.

The above is evidenced by the calculation of parameters for generation of initial melts based on glass compositions following the technique mentioned above [*Schilling et al.,* 1995]. Basalts from the Northern and the 3rd Southern domains (Station 1045) have uniform magma generation parameters with the shallowest depth (44–55 km) and lowest temperatures (1320–1370°C) for the entire Sierra Leone region. The "Ore area" and the Markov Basin are characterized by broad variations and maximum depths (45–78 km) and temperatures (1330–1450°C) of mantle melting. It can be noted that magmatic systems adjoining areas with sulfide mineralization are distinguished by a somewhat unusual combination of high temperatures with minimum depths. Station 1037 basalts (characterizing the Southwest domain) have similar magmagenesis conditions. Therefore, the mantle plume expands dramatically the melting interval, leading to diversity of melting conditions and involving underlying mantle horizons in the melting process.

The above implies an extremely uncommon combination of conditions for the genesis and evolution of basaltic melts in sulfide-bearing structures—the Markov Basin and the "Ore area." These structures develop and exist in tectonically unstable conditions due to spreading processes being overprinted by transtensional stresses. This tectonic instability manifests itself at the level of the magma generation zone, but at the crustal level the character of movements is such as to give rise to a tectonically stable zone, where relatively long lived intermediary magma chambers are formed and exist. This is evidenced by the fact that precisely these structures accommodate the most evolved basalt suites, associated with gabbroic series evolved to plagiogranite inclusive. These same domains are located in the zone of fluid flows traveling from deep mantle plumes, to enrich initial melts in lithophile elements and, probably, mineralizing components. The proximity of mantle plumes also results in migration of the high temperature region to a shallower level. Apparently, it is joint effect of all these factors that initiates sulfide-mineralizing hydrothermal plumbing systems within structures under study. The long term existence of a magma chamber maintains the functioning of a high-temperature hydrothermal system. Differentiation processes in the magma chamber result in high contents of mineralizing phase in the last portions of the melt, from where this phase jointly with fluid may be supplied to the hydrothermal plumbing system. One of the sources of elevated abundances of the ore phase may be deep plume material contributed to basaltic melts in one or another form.

It is worthwhile to note that Sierra Leone basaltic volcanism has many features in common with that in the southern near-FZ domain of the Cape Verde FZ region. These features include: active volcanism combined with, and dominated by, vigorous tectonism; widespread plutonic magmatism; broad occurrence of high-Mg basalt varieties; the presence of alkaline basalts at the ridge flanks and enriched tholeiites in rift-related structures [*Skolotnev et al.,* 1999]. Because both regions display massive sulfide mineralizations, it follows that all the above features may serve as exploration guides to such mineralization.

Conclusions

(1) Three sharply dissimilar basaltic varieties are discriminated. Broad, nearly ubiquitous occurrence is shown by high-Mg basalts that are derivatives of N-MORB-like tholeiitic melts originating beneath the rift valley in the axial zone of spreading. Another variety is alkaline basalts widespread on the southwest flank of the crestal zone of the Sierra Leone region and likely originating through melting in a deep mantle plume. Evidence has been found that plume activity takes place at the eastern flank of this region as well. A third variety is basalts derivative from T- and P-MORB-like tholeiitic melts and resulting from addition of deep mantle plume material to depleted melts. Magmagenesis parameters, as calculated from chilled glass compositions, suggest different magmagenesis conditions for depleted tholei-

ites (44–55 km, 1320–1370°C) and enriched tholeiites (45–78 km, 1330–1450°C).

(2) Not only do mantle plumes exert influence on compositions of tholeiitic rift-related basalts, leading to their enrichment in lithophile elements (T- and P-MORB-like basalts), but they also affect basalt magmagenesis conditions, resulting in stronger Ti and Na enrichment of melts initial to rift-related basalts in the vicinity of the plumes. T- and P-MORB-like basalts are also widespread near plume regions.

(3) Among the high-Mg basalts, discriminated are several types according to their titanium and sodium contents. Virtually each particular MAR segment in the study region, bounded by sinistral strike slips and the Bogdanov FZ, is characterized by such basalt type of its own, suggesting that every such segment is formed above a diapiric high of the asthenosphere with its unique magmagenesis conditions. These conditions change with time. The likely underlying causes for the temporal and spatial instability of mantle upwelling beneath the axis of this MAR region is singular tectonic processes and mantle plume activity.

(4) The high-Mg basalts are poorly evolved. It is only in sulfide-bearing structures (the "Ore area," the Markov Basin) that basalts constitute highly evolved suites resulting from fractional crystallization of olivine and plagioclase. Association of evolved basaltic suites with evolved gabbroic ones suggests that beneath the sulfide-bearing structures there exist relatively long lived magma chambers.

(5) The mineral potential of the rift-related structure developed in this region of the MAR is due to interplay of several tectono-magmatic processes and factors. It is owing to the tectonic stability of limited portions of the rift, occurring within the temperature impact from a mantle plume, that beneath these domains of the rift there comes into being an intermediary, relatively long lived magma chamber. Melts that undergo profound differentiation in this magma chamber have been variably affected by deep mantle plume material. Differentiation processes lead to progressively increasing concentration of the mineral phase, ultimately to be supplied to the hydrothermal plumbing system.

Acknowledgments. This work was carried out in compliance with the World Ocean Governmental Program under the financial support from the Russian Federation Ministry of Industry, Science, and Technologies and the Russian Foundation for Basic Research (grant nos. 00-05-64235, 02-05-64046, 02-05-64652).

References

Ariskin, A. A., and G. S. Barmina, *Modeling Phase Equilibria during Basaltic Magma Crystallization,* 363 pp., Nauka, MAIK "Nauka/Interperiodika," Moscow, 2000.

Ariskin, A. A., M. Ya. Frenkel, G. S. Barmina, and R. L. Nielsen, COMAGMAT: a Fortran program to model magma differentiation processes, *Computers & Geosciences, 19,* (8), 1155–1170, 1993.

Bogdanov, Yu., N. Bortnikov, I. Vikent'ev, E. Gurvich, and A. Sagalevich, A new type of modern mineral-forming systems: "black smokers" of the hydrothermal field at 14°45′ N, Mid-Atlantic Ridge (in Russian), *Geol. Rudn. Mestorozhd., 39,* (1), 68–90, 1997.

Bonatti, E., Ultramafic Rocks from the Mid-Atlantic Ridge, *Nature, 218,* (5152), 363–364, 1968.

Dosso, L., B. B. Hanan, H. Bougault, et al., Sr-Nd-Pb geochemical morphology between 10° and 17°N on Mid-Atlantic Ridge: a new MORB isotope signature, *Earth Planet. Sci. Lett., 106,* (1), 29–43 1991.

Bazilevskaya, E., and S. Skolotnev, Fe–Mn crusts in the Sierra Leone FZ region (equatorial Atlantic) (in Russian), *Dokl. Ross. Akad. Nauk, 383,* (6), 791–795, 2002.

Evensen, N. M., P. J. Hamilton, and R. K. O'Nions, *Geochim. et Cosmochim. Acta, 42,* 1199–1212, 1978.

Irvine, T. N., and W. R. A. Baragar, A guide to the chemical classification of the common volcanic rocks, *Canadian J. Earth Sci., 8,* 523–548, 1971.

Klein, E. M., and Ch. H. Langmuir, Global correlations of ocean ridge basalt chemistry with axial depth and crustal thickness, *J. Geophys. Res., 92,* (B8), 8089–8115, 1987.

Mazarovich, A., and S. Sokolov, Tectonic position of the hydrothermal fields of the Mid-Atlantic Ridge (in Russian), *Litol. Polezn. Iskop., 4,* 436–439, 1998.

Mazarovich, A., V. Simonov, A. Peyve, S. Kovyazin, G. Tret'yakov, Yu. Raznitsyn, G. Savelieva, S. Skolotnev, S. Sokolov, and N. Turko, Hydrothermal mineralization in Sierra Leone Fracture Zone (Central Atlantic) (in Russian), *Litol. Polezn. Iskop., 5,* 1–8, 2001a.

Mazarovich, A., K. Dobrolyubova, V. Efimov, S. Sokolov, and N. Turko, Bogdanov Fracture Zone, Central Atlantic: The first description (topography and sediments) (in Russian), *Geotektonika, 6,* 75–83, 2001b.

Mazarovich, A. O., S. Yu. Sokolov, N. N. Turko, and K. O. Dobrolyubova, Bathymetry and structure of the rift zone of the Mid-Atlantic Ridge between 5° and 7°18′ N, *Russian Journal of Earth Sciences, 3,* (5), 2001c (electronic version, www.agu.org/wps/rjes).

Niu, Ya., and R. Batiza, Magmatic processes at slow spreading ridge segment: 26°S Mid-Atlantic Ridge, *J. Geophys. Res., 99,* (B10), 19719–19740, 1994.

Peyve, A., K. Dobrolyubova, V. Efimov, A. Cipriani, M. Liggi, A. Mazarovich, A. Perfil'ev, Yu. Raznitsin, G. Savel'eva, V. Simonov, S. Skolotnev, S. Sokolov, and N. Turko, Structural features of the Sierra Leone FZ region (Central Atlantic) (in Rusian), *Dokl. Ross. Akad. Nauk, 377,* (6), 803–806, 2001.

Pushcharovsky, Yu. M. (Ed.), *Architecture of the Cape Verde FZ: Central Atlantic,* 199 pp., Nauka, Moscow, 1989.

Pushcharovsky, Yu., Yu. Raznitsin, A. Mazarovich, S. Skolotnev, P. Kepezhinskas, N. Turko, A. Peyve, and D. Dmitriev, The Arkhangelsky, Doldrums, and Vernadsky Fracture Zones, Central Atlantic: Structure and Lithology (in Russian), *Geotektonika, 6,* 63–79, 1992.

Pushcharovsky, Yu., N. Bortnikov, S. Skolotnev, A. Peyve, V. Kolobov, N. Tsukanov, S. Lyapunov, E. Sharkov, A. Mochalov, M. Stolyarov, D. Krinov, N. Razdolina, and A. Cipriani, Massive and stringer–disseminated sulfide mineralization on the Mid-Atlantic Ridge in the Sierra Leone FZ region in connection with its geologic structure (in Russian), *Dokl. Ross. Akad. Nauk, 384,* (1), 83–88, 2002.

Sandwell, D. T., and W. H. V. Smith, Marine gravity anomaly from Geosat and ERS 1 satellite altimetry, *J. Geophys. Res., 102,* 10,039–10,054, 1997.

Schilling, J., B. Hanan, B. McCully, R. H. Kingsley, and D. Fontignie, Influence of the Sierra Leone mantle plume on the equatorial Mid-Atlantic Ridge: A Nd-Sr-Pb isotopic study, *J. Geoph. Res., 99,* (B6), 12,005–12,028, 1994.

Schilling, J.-G., C. Ruppel, A. N. Davis, B. McCully, S. A. Tighe, R. H. Kingsley, and J. Lin, Thermal structure of the mantle beneath the equatorial Mid-Atlantic Ridge: Influences from the spatial variation of dredged basalt glass compositions, *J. Geophys. Res., 100,* (B7), 10,057–10,076, 1995.

Skolotnev, S., Gabbroic rocks of the Vema Fracture Zone: Textures, composition, and tectonic setting (in Russian), *Petrologiya, 11,* (1), 18–31, 2003.

Skolotnev, S., A. Peyve, and S. Lyapunov, Tectono-volcanic activity in the crestal part of the Mid-Atlantic Ridge between the Cape Verde and Mercury FZs (Central Atlantic) (in Russian), *Petrologiya, 7,* (6), 591–610, 1999.

Sun, S. S., R. W. Nesbit, and A. Ya. Sharaskin, Geochemical characteristics of mid-ocean ridge basalts, *Earth Planet. Sci. Lett., 96,* 119–133, 1979.

Udintsev, G., N. Kurentsova, A. Kol'tsova, A. Knyazev, D. C. Hall, and V. Udintsev, Bathymetry and architecture of the equatorial segment of the Mid-Atlantic Ridge (in Russian), *Okeanologiya, 36,* (6), 897–909, 1996.

(Received 16 April 2003)